



Comparative analysis of hydrodynamics of treatment wetlands using finite volume models with empirical data

Rattandeep Singh^{a,*}, Sandeep Gupta^a, S. Raman^b, Prodyut Chakraborty^a, Puneet Sharma^a, Rakesh Kumar Sharma^a, Larry C. Brown^c, Xiaohua Wei^d, Anand Plappally^a

^aIndian Institute of Technology Jodhpur, Old Residency Road, Ratanada, Jodhpur, Rajasthan 342001, India, Tel. +91 8384920551; email: PG201271005@iitj.ac.in (R. Singh)

^bElectrical Engineering, Indian Institute of Technology Gandhinagar, Gandhinagar, Gujrat, India

^cFood, Agricultural and Biological Engineering Department, The Ohio State University, Columbus, OH, USA

^dDepartment of Civil and Environmental Engineering, Nanyang Technological University, Singapore

Received 1 April 2014; Accepted 16 June 2014

ABSTRACT

A numerical visualization study of wetlands is detailed in this article using finite volume methods. The aim of this study is to model treatment efficiency of the wetlands in terms of the residence time distribution function. Shape and depth of wetlands are critically analysed to find the optimal flow requirement for effective treatment. Laminar three-dimensional flow dynamics is used to simulate the slow water flows that occur in treatment wetlands. Slow inlet flows are assumed. Dye is used as the tracer to characterize the hydrodynamics within the wetlands. Three different geometrical configurations, namely square, square with two islands, and triangle, respectively, are simulated. The variation in the tracer concentration is studied as a function of recirculation volumes, flow rates, time and depth of the wetland for each of the wetland shapes. The change in the variation of tracer concentration at inlet and exit helps to assess treatment effectiveness. In another case, glycerine is used to simulate sewage flow. Plug flow is prominent in sewage-laden wetlands. The results obtained from the above-illustrated case studies are compared with each other to assess the reproducibility of the optimal flow model. Multi-parameter regression models for residence time distribution functions are derived to characterize flow through constructed wetlands of different shapes.

Keywords: Wetlands; Shape; Depth; Numerical; Residence time; Visualization; Tracer; Dye

1. Introduction

Wetlands can be seen in almost all regions in India but are generally neglected and misused. They are an

integral part of nature and act as natural water treatment plants. These are shallow waters which are the closest transition between terrestrial and aquatic ecosystems [1].

Wetlands help in preventing floods [2]. They retain water during dry periods, thereby maintaining a high

*Corresponding author.

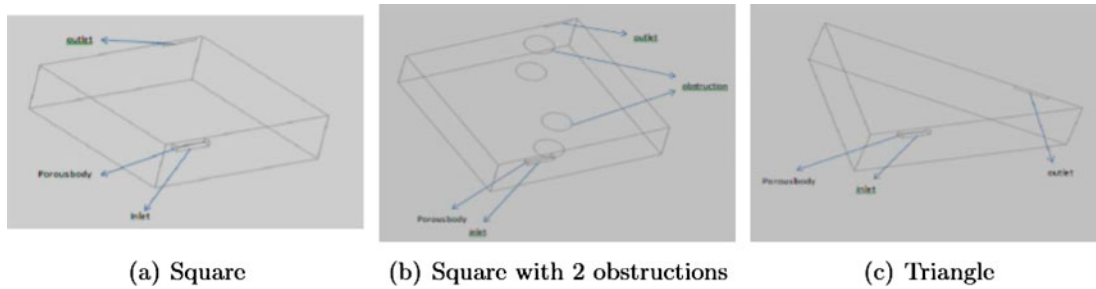


Fig. 1. Three-dimensional plots of the three different wetland configurations (square, square with two islands, and triangle, respectively) tested and numerically analysed.

Table 1
Energy consumed for the treatment of wastewater [4]

Wastewater treatment	Equivalent energy intensity (kWh/m ³)
Lagoon	0.09–0.29
Trickling filter	0.18–0.42
Activated sludge	0.33–0.60
Advanced wastewater treatment	0.31–0.40

ground water level [2]. They trap sediments and nutrients and hence prevent them from going into connected large water bodies [2]. They help in water treatment by carrying out functions like sedimentation, decomposing vegetative matter and converting chemicals into useable form [1].

Biological activities are more dominating in wetlands [2]. Wetland land area, plants present in it, microclimate, soil and solar radiations together help in the biological degradation of these waste materials [1–3].

1.1. Why wetlands are important in the water treatment process

According to Plappally et al. [4], the energy intensities (electrical) of secondary wastewater treatment processes in the USA are as follows [4]:

Lagoons are wetlands which reduce the larger molecular and nitrate impurities in the secondary level water treatment [4]. It is found that lagoons provide treatment at the expense of less energy per cubic metre of water. As wetlands have the natural ability to treat water, the wastewater from agricultural lands or industries can be recycled thereby reducing the cost expended on water [4]. According to Gollehen et al., in the USA, for carrying out irri-

Table 2
Shape, height and flow rate used

Shape	Height (cm)	Wetland inflow rate (ml/min)
Square	15.5	150
		300
	31	150
		300
	45.5	300
		500
Square with two obstructions or islands	15.5	150
		300
	31	150
		300
	45.5	300
		500
Triangle	15.5	150
		300
	31	150
		300
	45.5	300
		500

gation processes, approximately 12775.4e⁰⁶ US dollars, 278.72e⁰⁶ US dollars, 578.75e⁰⁶ US dollars and 491.77e⁰⁶ US dollars are spent annually for

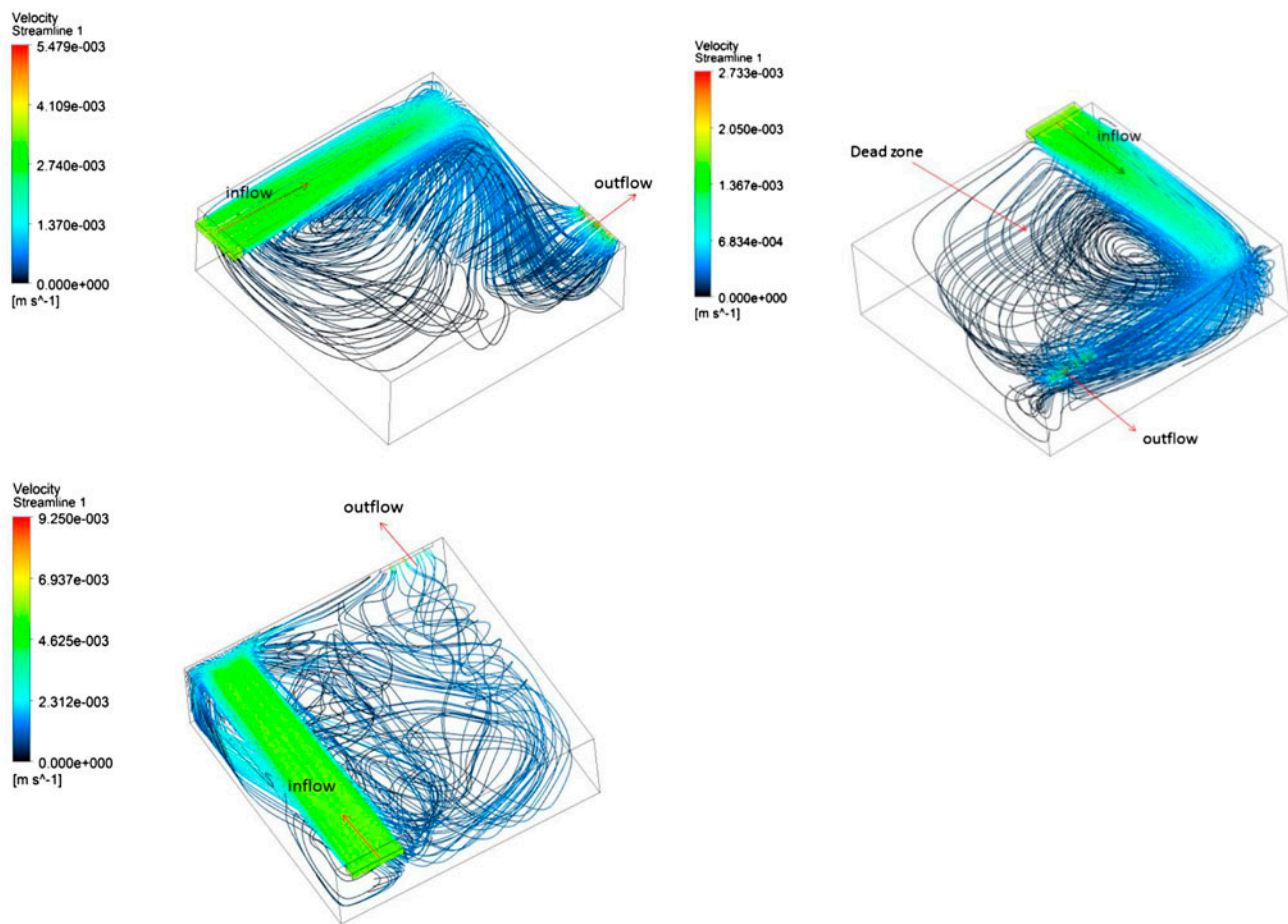


Fig. 2. Streamlines at different volumetric flow rates (150, 300 and 500 ml/min, respectively) for square shape at a height of 15.5 cm.

groundwater pumping, surface water pumping, procuring water from other sources and carrying out maintenance and repair of treatment and supply systems, respectively [5]. These costs can be reduced to a large extent if proper care is taken in the conservation of wetlands. Constructed wetlands used for the treatment of produced water from oil wells and shales only cost a minimum of 0.006 \$/m³ [6].

The hydraulic efficiency of wetlands depends upon wetland shape, water height or head, wastewater inflow rate and climatic and soil conditions [2–10]. In this paper, only hydraulic conditions are taken into account, and parameters like evapotranspiration, rainfall and infiltration are neglected. Computational models of the wetlands are developed and their effect on hydraulic efficiency is determined in this study.

Fan et al. [8] carried out computational fluid dynamics (CFD) simulations to determine how distribution and catchment area affect the hydraulic performance of subsurface flow wetlands. In this, two-dimensional models of wetlands were developed and simulations were carried out to determine how hydraulic efficiency gets affected by the horizontal or vertical distributions or catchment area. From their study, they found that hydraulic efficiency of wetlands can be very low if the horizontal distribution or catchment area is not selected appropriately [8]. They also found that hydraulic efficiency of wetlands changes very slightly with change in vertical distribution and/or catchment area. Also, they concluded that the efficiency of vertical distribution and/or catchment area in subsurface flow wetlands is more than that of horizontal distribution and/or catchment area [7].

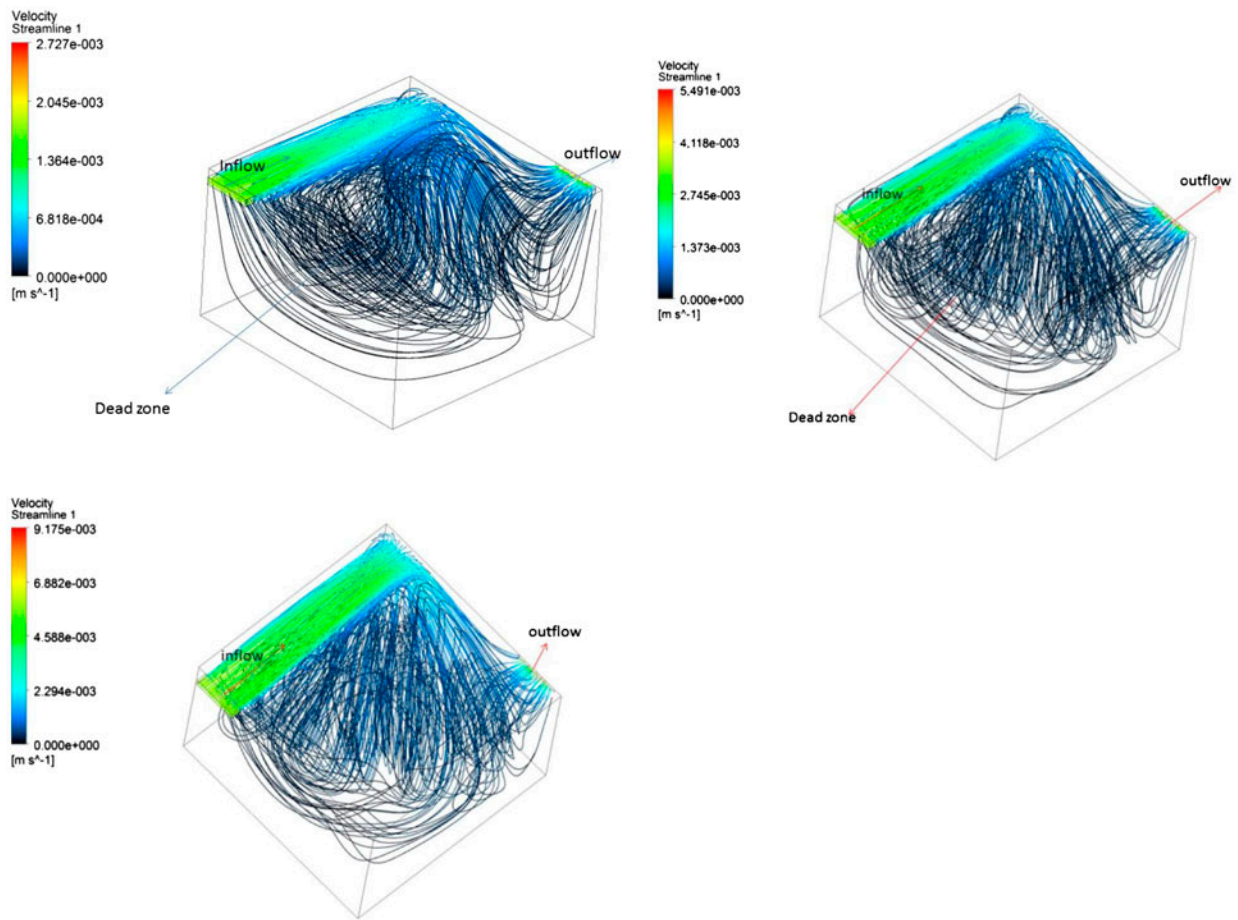


Fig. 3. Streamlines at different volumetric flow rates (150, 300 and 500 ml/min, respectively) for square shape at a height of 31 cm.

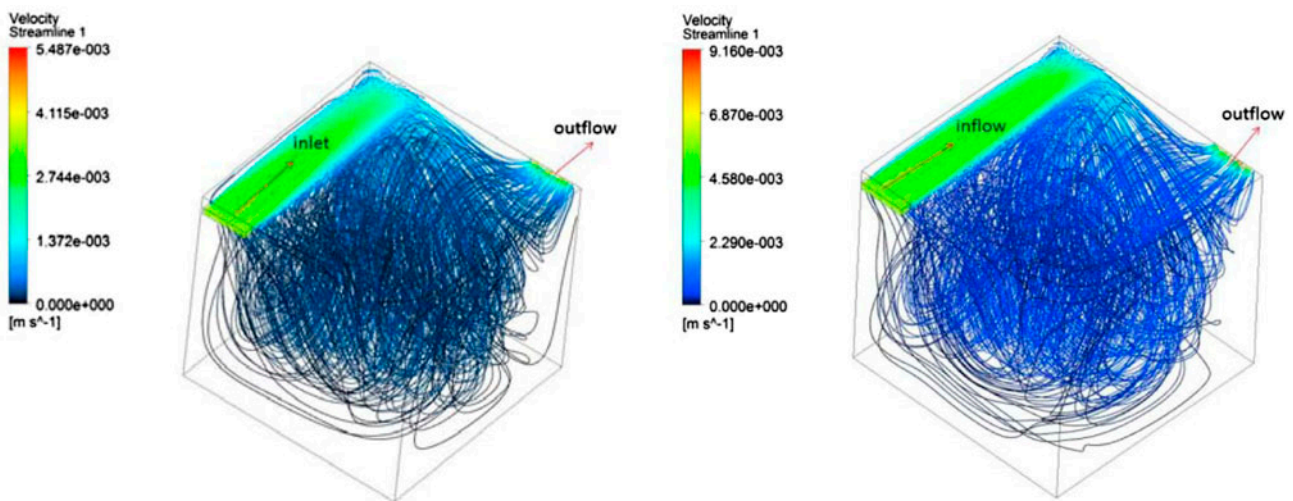


Fig. 4. Streamlines at different volumetric flow rates (300 and 500 ml/min, respectively) for square shape at a height of 45.5 cm.

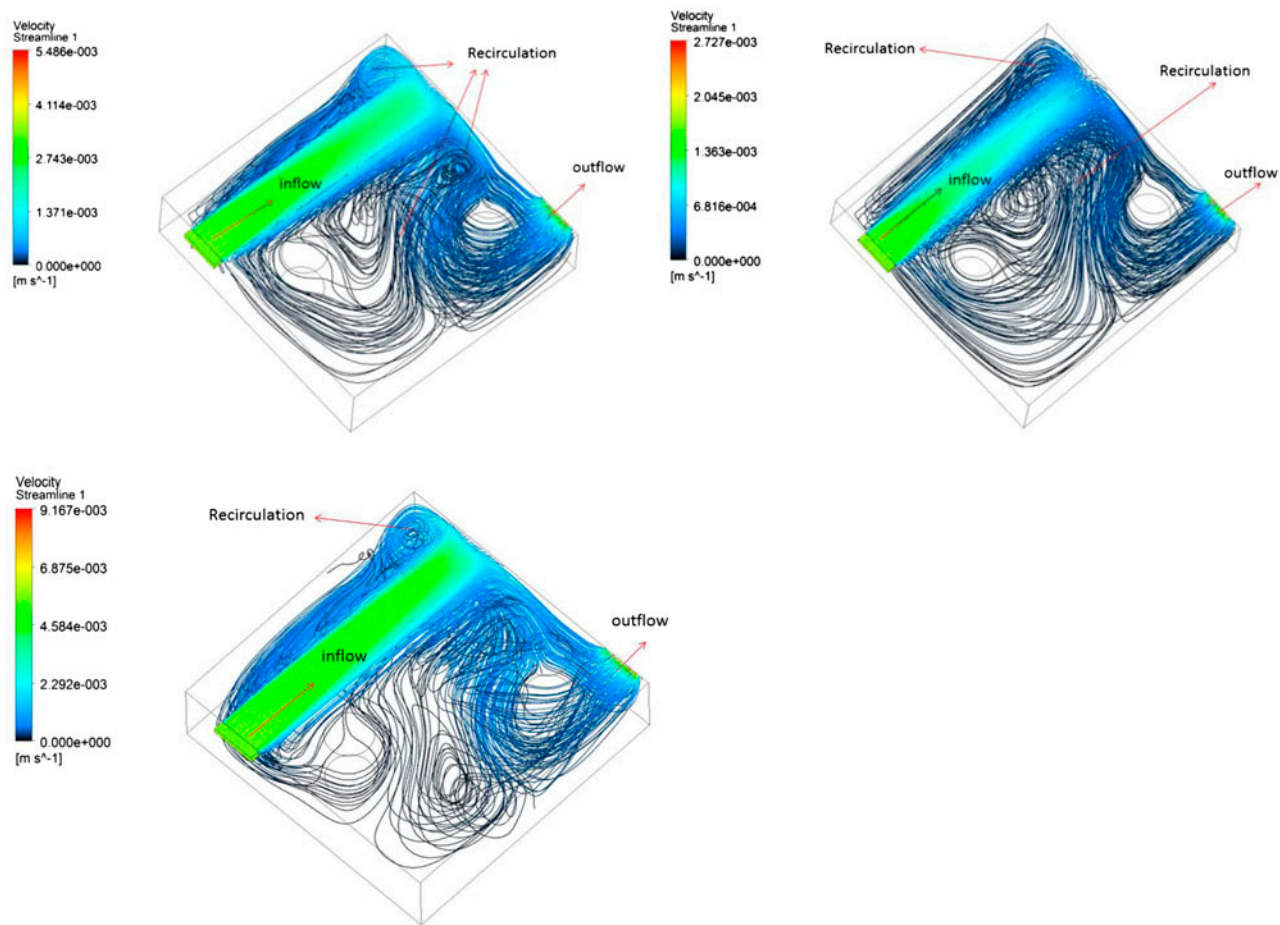


Fig. 5. Streamlines at different volumetric flow rates (150, 300 and 500 ml/min, respectively) for square shape having two islands at a height of 15.5 cm.

Fan et al. [8] also carried CFD simulations on subsurface flow wetlands to determine how the inlet position and protection media affects the hydraulic efficiency of wetlands. They varied the position of inlets and determined that with change in the position of inlets, the hydraulic efficiency of wetlands changes. Fan et al. [8] divided the subsurface flow wetlands into two regions: upper constructed media and lower constructed media, and using simulations, determined the effect of constructed media on hydraulic efficiency. They also determined that although there is an increase in hydraulic efficiency of treatment wetlands with increase in velocity, hydraulic performance decreases as the residence time of impurities decreases due to increase in flow velocity. Therefore, a balance is to be maintained in case of velocity [8].

Persson [9] used two-dimensional numerical techniques to determine how the hydraulic efficiency

of 13 different shapes of ponds changes with inlet and outlet positions and with length to width ratio. Persson [9] also studied how hydraulic efficiency gets affected by the presence of islands (in wetlands). With the addition of an island or an obstruction in the path of water, short-circuiting decreases, the effective volume of the wetland increases and there is a decrease in the amount of mixing [9]. Furthermore, his study showed that the inlet–outlet position and the ratio of length to width also contribute towards the hydraulic performance of the ponds, and although increasing the length to width ratio decreases short-circuiting, the same can be attained by placing an island in the path of water [9].

In India, small farmlands are common. In Guilin, China, experimental farmland-channel-wetland-systems (FCWS) have been developed for small farms which are based on wetland water reuse

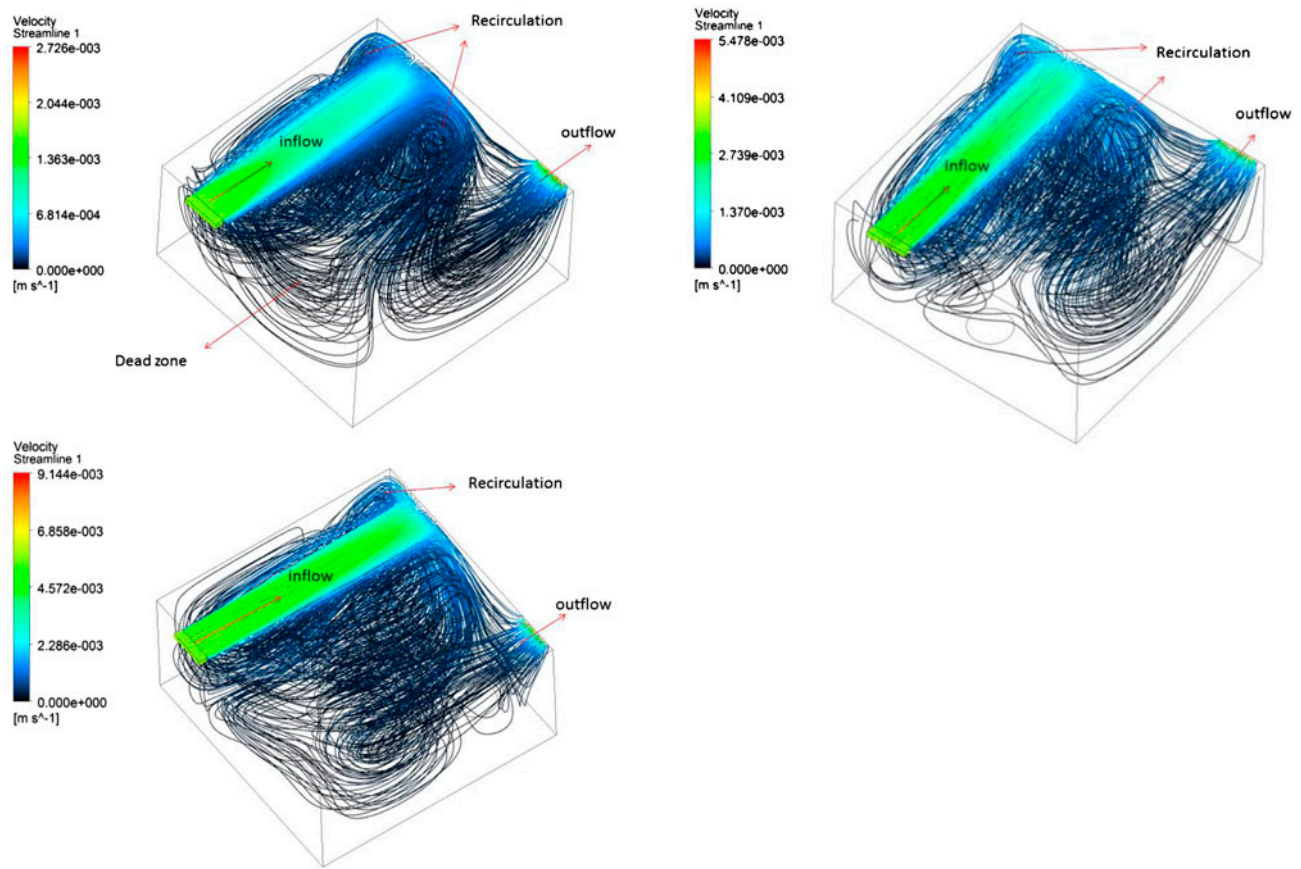


Fig. 6. Streamlines at different volumetric flow rates (150, 300 and 500 ml/min, respectively) for square shape having two islands at a height of 31.0 cm.

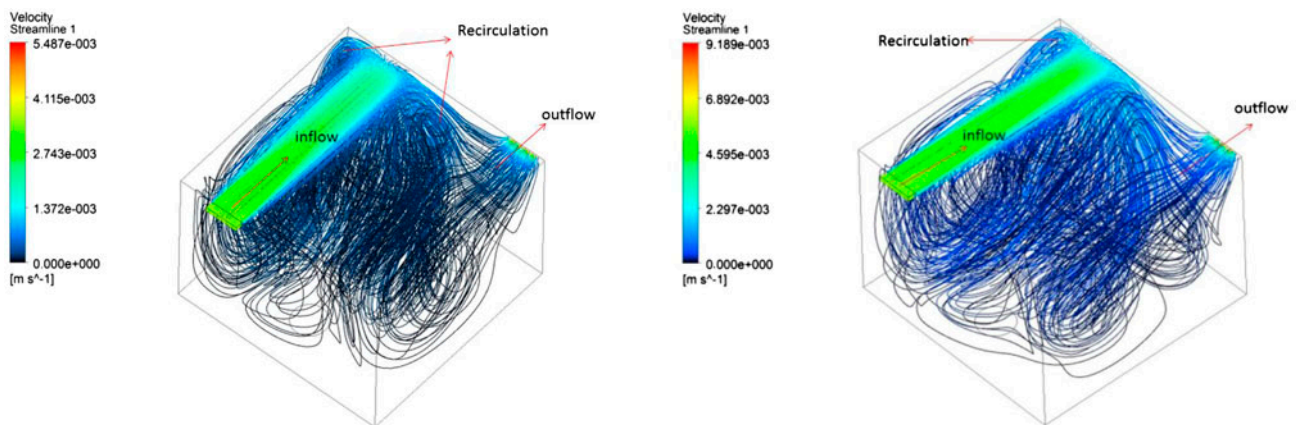


Fig. 7. Streamlines at different volumetric flow rates (300 and 500 ml/min, respectively) for square shape having two islands at a height of 45.5 cm.

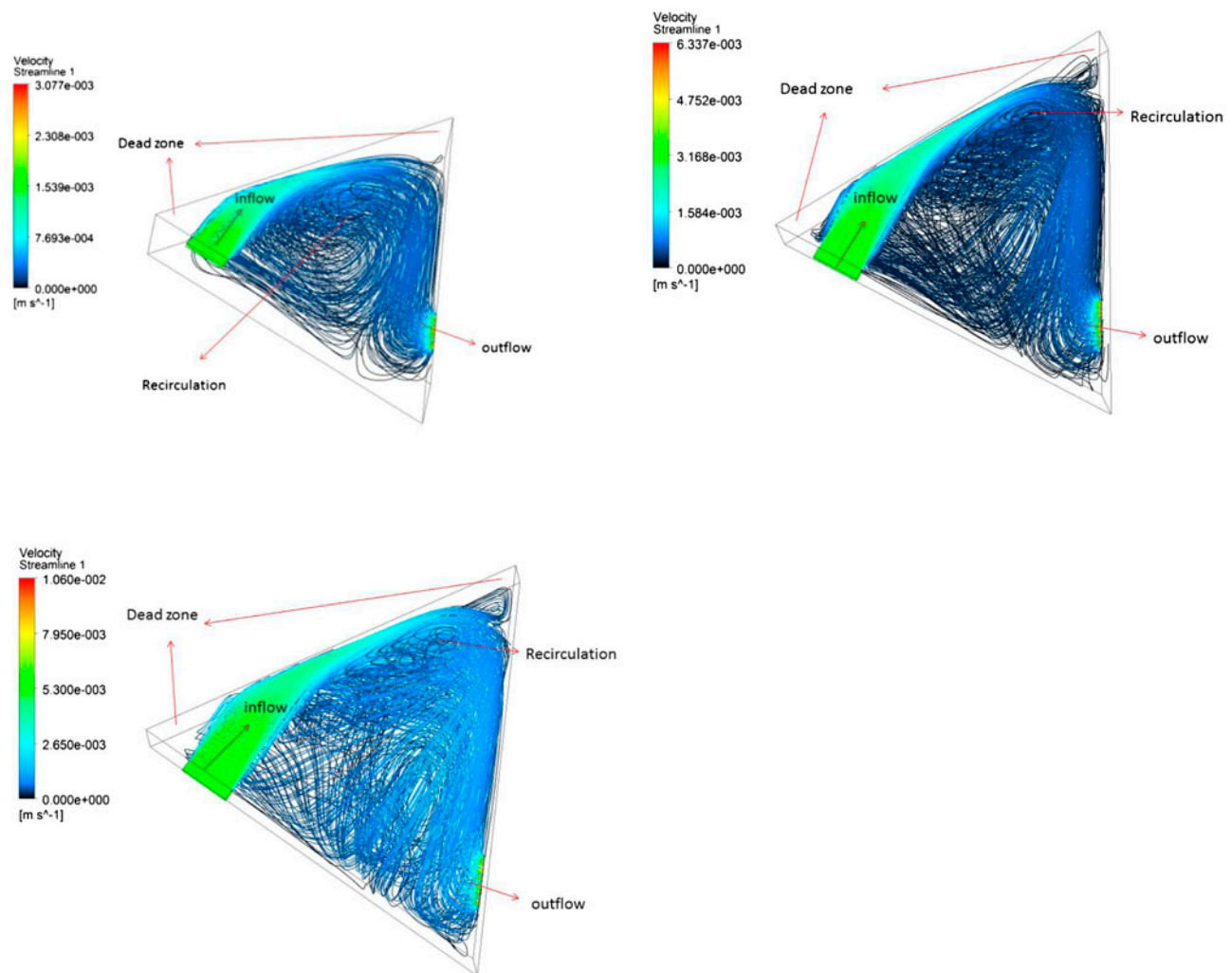


Fig. 8. Streamlines at different volumetric flow rates (150, 300 and 500 ml/min, respectively) for triangular shape at a height of 15.5 cm.

systems in Midwest USA [10]. Wei et al. [10] performed simulations on various two-dimensional shapes of these FCWS wetlands and modelled an approach in which residence time can be written as a function of shape, mass inflow and inlet geometry [10,11].

In the present study, simulations are carried out for free surface flow wetlands, and consist of two major aspects. First is the hydrodynamic analysis of the three-dimensional wetland models with negligible flow velocities [12–14]. This is conducted taking into consideration three different geometrical constructed designs of wetlands. These geometries are discussed in the following section elaborately. Suitable variability in the residence time distribution will be studied. The variability is assessed with

respect to the recirculation or dead zones within the wetland [11,15]. The density of recirculation zones may provide the efficiency of the treatment by the wetland through probable techniques of sedimentation. It is evident that dead zones are areas of negligible velocities which may promote settling down of impurities or increase the contact time of impurities helping them to agglomerate [15]. The viability of change in the head of the wetland is also taken into consideration to account optimal design of the wetland [11].

In the second part, sewage wastewater treatment using wetlands is considered. Glycerine has properties simulating the high suspended solids and viscosity of sewage slurry [16]. Plug flow may take place within the sewage flow zones [16]. In the second part of the

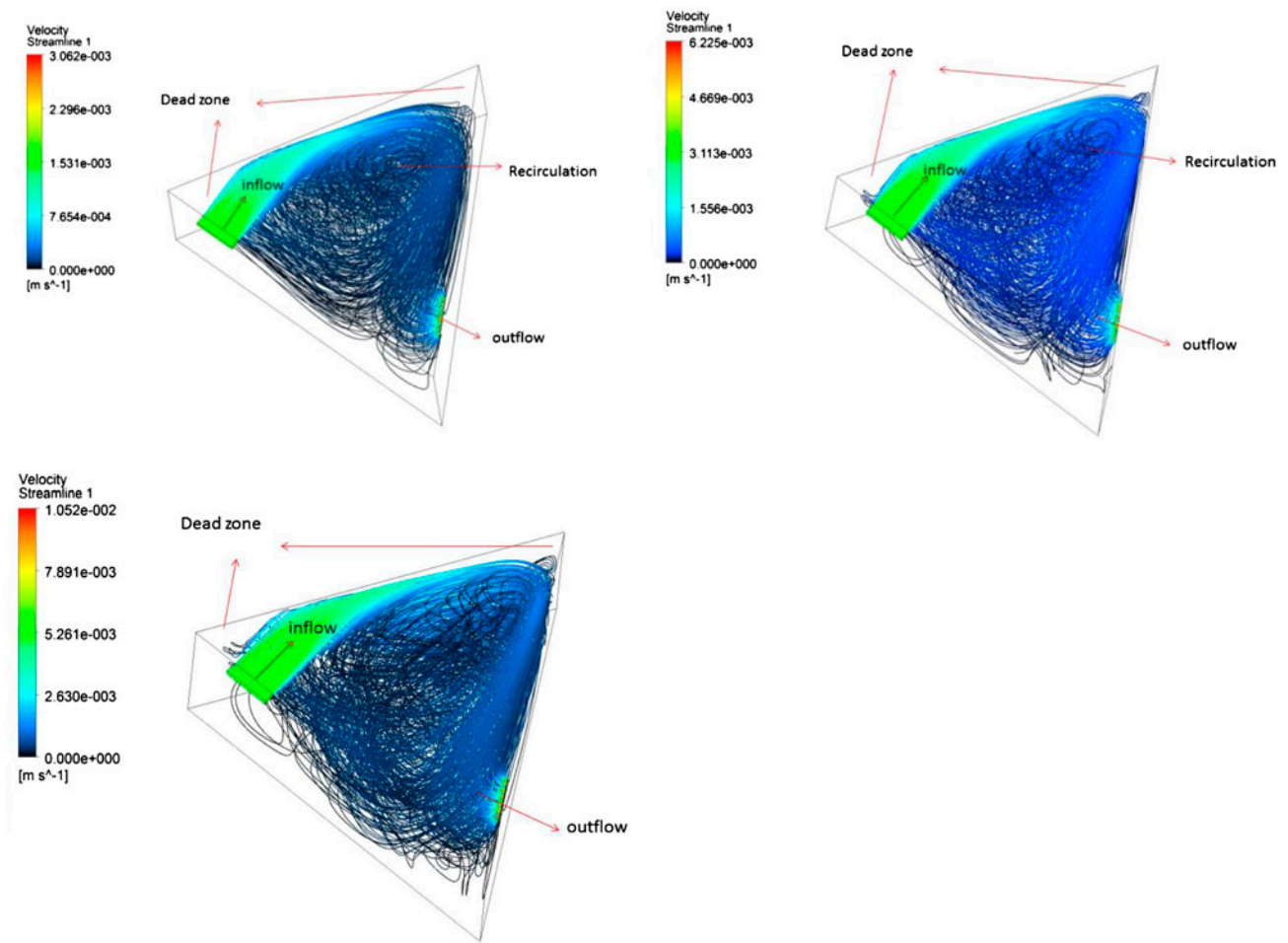


Fig. 9. Streamlines at different volumetric flow rates (150, 300 and 500 ml/min, respectively) for triangular shape at a height of 31.0 cm.

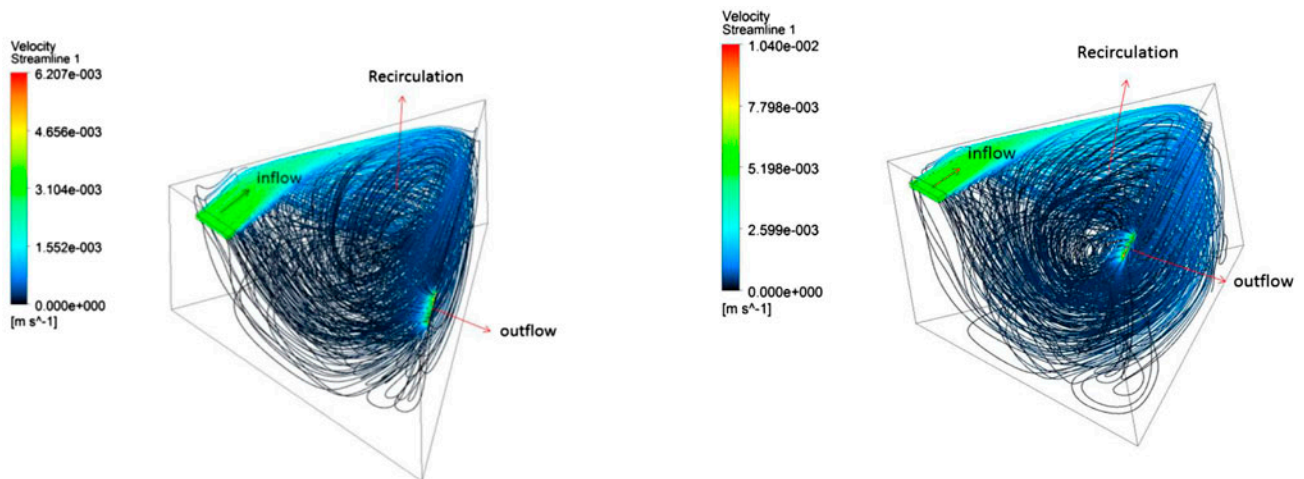


Fig. 10. Streamlines at different volumetric flow rates (300 and 500 ml/min, respectively) for triangular shape at a height of 45.5 cm.

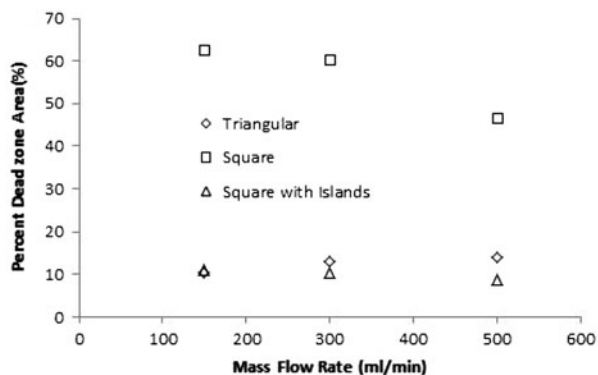


Fig. 11. Variation of dead zones in wetlands of different velocities for three different geometric configurations at a head of 15.5 cm.

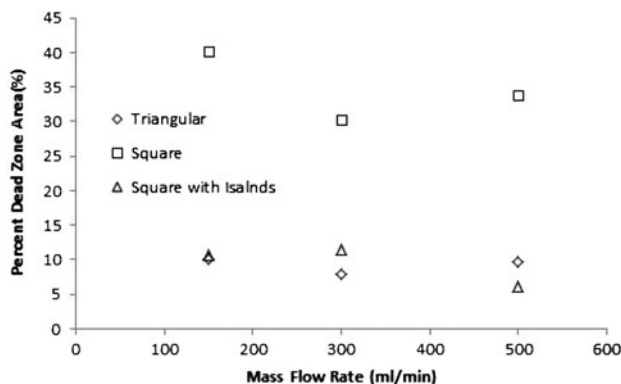


Fig. 12. Variation of dead zones in wetlands of different velocities for the three different geometric configurations at ahead of 31.0 cm.

study glycerine is used as the working fluid instead of water. The same assumptions as those in the numerical simulations performed in the first part were fol-

lowed. From these computations, the residence time distribution of waste matter through the sewage-type fluid can be determined.

Table 3

Hydraulic efficiency of the wetland shapes for different inflow rates along with different heights of water

Shape	Height (cm)	Flow rate	t_n	t_θ	t_{mean}	σ^2	λ	
Square	15.5	150	15,500	0.7954	12328.767	7.4e+07	0.5505	
		300	7,750	0.7633	5915.2688	9.97e+06	0.6365	
		500	4,650	0.7831	3641.399	5.26e+06	0.592	
	31	150	31,000	0.3105	9,628.565	3.79e+07	0.2983	
		300	15,500	0.65189	10104.409	4.33e+07	0.5344	
		500	9,300	0.59958	5,576.1241	8.67e+06	0.5394	
	45.5	300	22,750	0.49498	11260.991	5.81e+07	0.4394	
		500	13,650	0.5916	8,075.494	2.32e+07	0.518	
	Square with islands	15.5	150	16,126	0.5268	8,496.41	2.67e+07	0.4727
300			8,063	0.7315	5,898.5119	9.9e+06	0.62014	
500			4,838	1.048	5,073.931	7.13e+06	0.7292	
31		150	32252.4	0.4834	15593.195	1.35e+08	0.421	
		300	16,126	0.501	8,171.787	2.39e+07	0.46	
		500	9,676	0.65	6,282.1812	1.16e+07	0.5687	
45.5		300	23,669	0.623	14754.139	1.18e+08	0.4924	
		500	14,201	0.956	13576.3	9.51e+07	0.505	
Triangle		15.5	150	15,506	0.382	5,919.45	9.99e+06	0.366
			300	7,753	0.8895	6,896.447	1.49e+07	0.6688
			500	4,652	0.8951	4,163.823	5.511e+06	0.6671
		31	150	31,012	0.2855	8,855.378	3.0e+07	0.2766
	300		15,506	0.5537	8,587.037	2.75e+07	0.49	
	500		9,304	0.9215	8,573.641	2.74e+07	0.629	
	45.5	300	22,759	0.631	14356.36	1.1e+08	0.497	
		500	13,656	0.641	8749.12	2.9e+07	0.541	

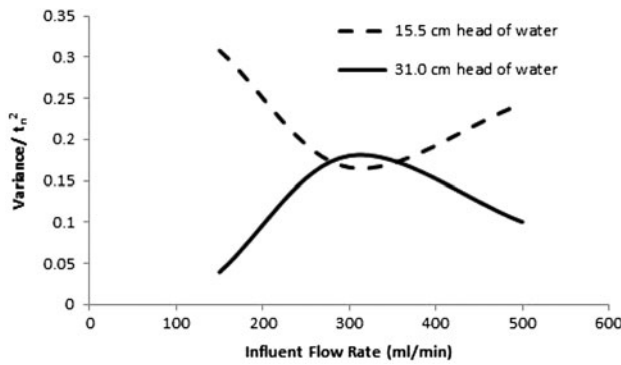


Fig. 13. The measure of mixing vs. flow velocity for square shape wetland hydrodynamics.

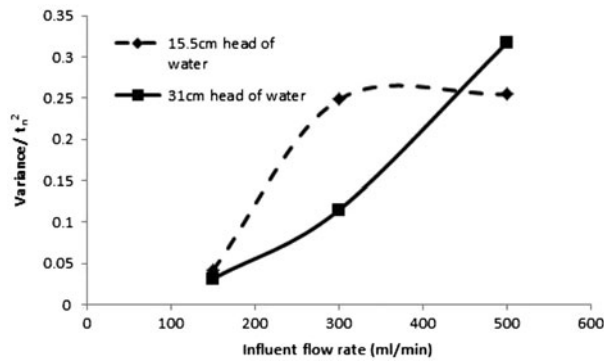


Fig. 14. The measure of mixing vs. flow velocity for triangular wetland hydrodynamics.

2. Mathematical model

2.1. Governing equations

The following equations govern the mass conservation equation of flow of fluid within the wetland [12,17]:

$$\frac{\partial u}{\partial x} + \frac{\partial v}{\partial y} + \frac{\partial w}{\partial z} = 0 \quad (1)$$

$$\rho \frac{D\mathbf{v}}{Dt} = -\frac{\partial p}{\partial x_i} + \nabla \cdot (\mu \nabla \mathbf{v}) + S_{M_i} \quad (2)$$

where ρ is the density of the fluid (in kg/m^3); u , v and w are the velocities along the x , y and z directions, respectively; \mathbf{v} is the velocity vector (in ms^{-1}); p is the static pressure; and S_{M_i} is the source term in the i th direction [12,17].

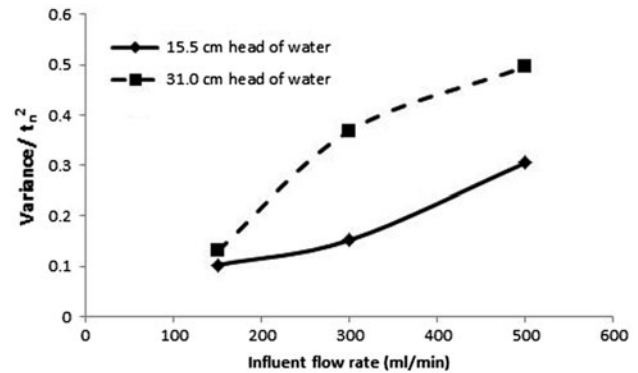


Fig. 15. The measure of mixing vs. flow velocity for square shape with two islands or obstructions.

In this case, there is a porous medium at the inlet geometry such that water enters the wetlands through this porous inlet. The porous medium is used to make sure that the flow entering the wetlands is plug flow. In case of homogenous porous media, S is given as [12]:

$$S = -\frac{\mu}{\alpha} \mathbf{v} + \frac{C_2 \rho \mathbf{v}^2}{2} \quad (3)$$

In case of laminar flow, the value of C_2 can be neglected [13], so the value of C_2 is taken to be zero. Face permeability of the porous medium was determined experimentally and its value was $7.5225 \times 10^{-9} \text{ m}^2$, while thickness of the porous medium was 2.2 cm. Since the thickness of the porous medium used was very less compared with the porous body while doing computations, a face was considered as a porous jump as shown in Fig. 1 [12].

For the first case of simulations, water was used as the working fluid; initially, each model was solved for steady state conditions [15]. Once the solution was converged using the velocity profile obtained through steady flow analysis, unsteady flow analysis of the tracer was performed [12,15]. The species transport model was used [13]. The equation used for the species transport model is given as [13]:

$$\frac{\partial \rho Y}{\partial t} + \nabla \cdot (\rho \mathbf{v} Y) = -\nabla \cdot \mathbf{J} \quad (4)$$

where Y is the mass fraction of each species and \mathbf{J} is the diffusion flux of the species [13]. For the unsteady analysis, the mass fraction of the species at

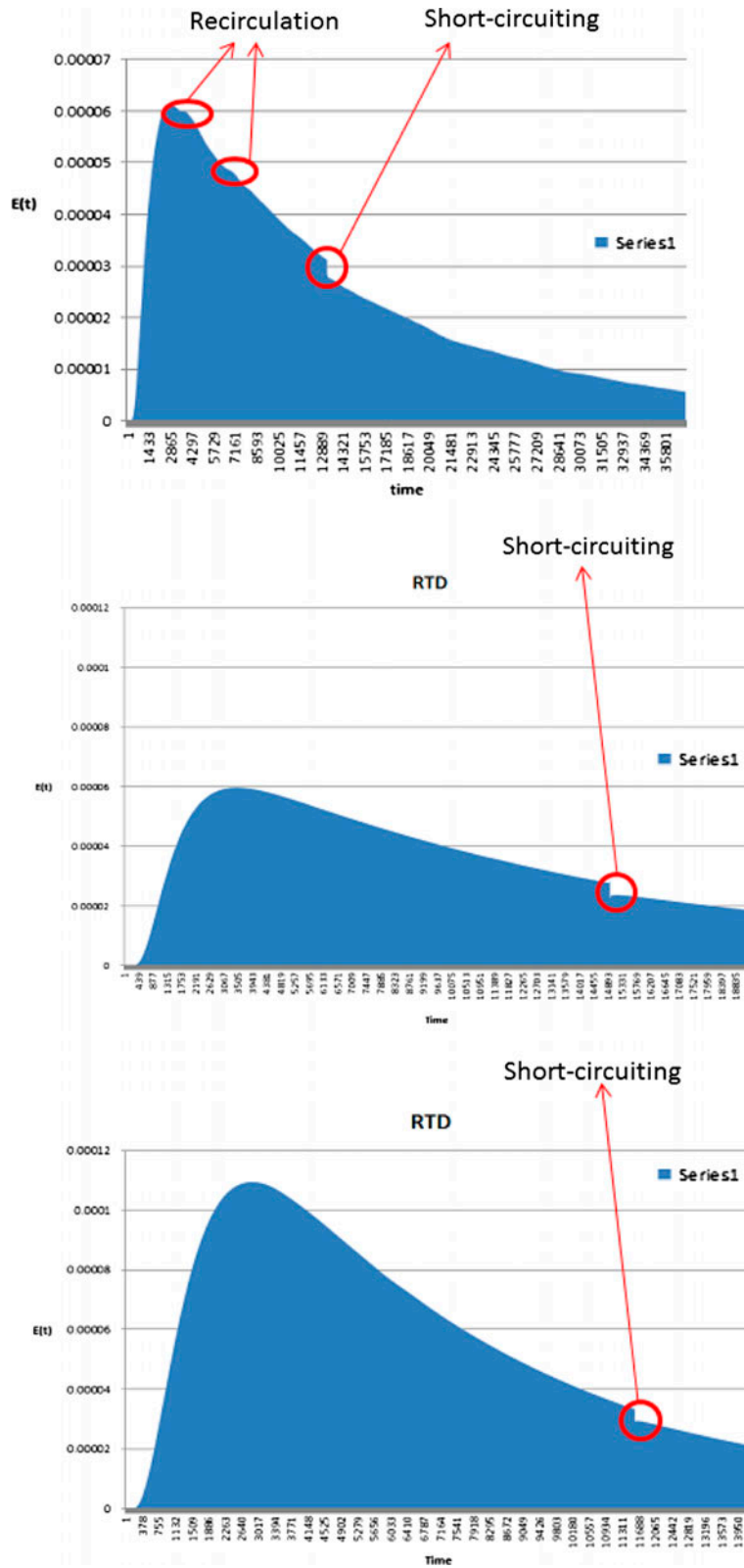


Fig. 16. Residence time distribution curves for the three geometries (square, square with two islands, and triangle, respectively) shown in Fig. 1, at a height of 15.5 cm and a flow rate of 150 ml/min.

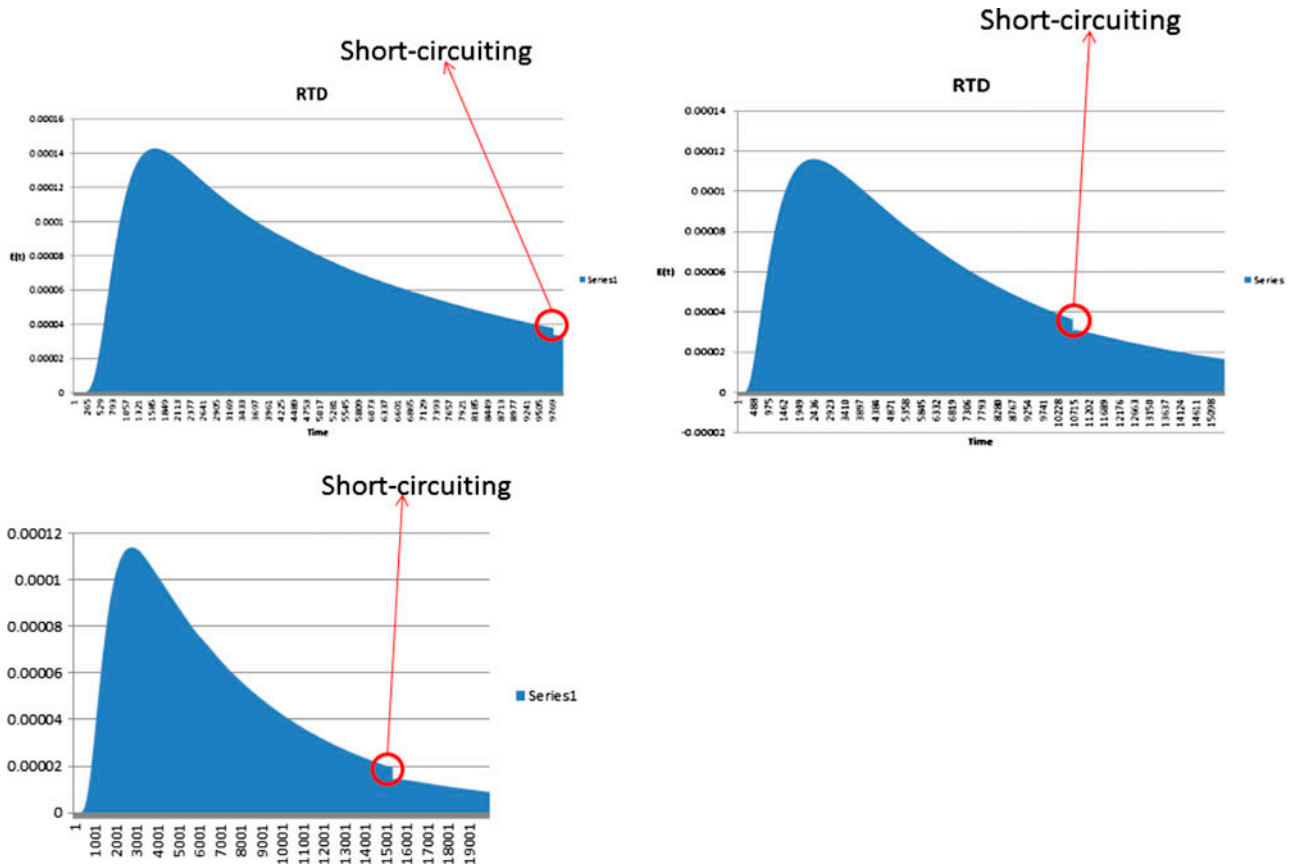


Fig. 17. Residence time distribution curves for the three geometries (square, square with two islands, and triangle, respectively) illustrated in Fig. 1 at a height of 15.5 cm and a flow rate of 300 ml/min.

the inlet was assumed to be unity, mass diffusivity or diffusion coefficient was equal to $2.88e^{-05}$ and density of the mixture was calculated using volume-weighted-mixing-law. The tracer from the inlet enters into the geometry by pure convection [12,13].

For the second part of the simulations in which glycerine was to be used as the working fluid, to determine the residence distribution time of species or waste particles inside the geometry, discrete phase modelling was used [13]. In this technique, particles were injected from the inlet into the model and the time taken by the particles to come out of the model was calculated by FluentTM to determine the residence distribution of particles inside the model. The following equations are used in the discrete phase model [18]:

$$\frac{du^p}{dt} = F_D(u - u^p) + g \left(\frac{\rho^p - \rho}{\rho^p} \right) + F \tag{5}$$

where $F_D = \frac{18\mu C_D R_e}{24\rho_p d_p^2}$, and $R_e = \frac{\rho^p |u - u^p|}{\mu}$. F_D is the drag force acting on the particle, ρ^p is the density of the injected particle and g is the acceleration due to gravity in that direction [18]. For the simulation of the flow of glycerine, wood particles were injected from the inlet such that the direction of flow of these wood particles is perpendicular to the direction of the inlet area. Initial velocity of wood particles is assumed to be zero. The density of wood is approximately 700 kg/m^3 [19].

2.2 Parameters used for determining hydraulic efficiency

Normalized retention time is the time fluid has spent inside the wetlands [14,20]. The larger the time, the better will be its treatment [14,17,20].

$$t_n = \frac{V_R}{V_o} \tag{6}$$

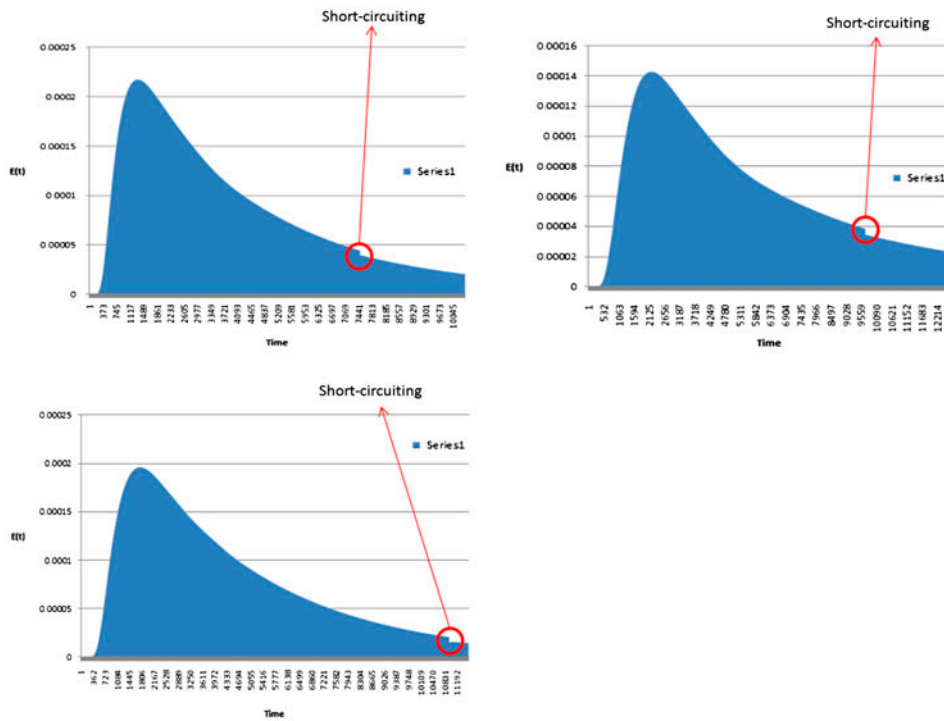


Fig. 18. Residence time distribution curves for the three geometries (square, square with two islands, and triangle, respectively) as shown in Fig. 1 at a height of 15.5 cm and a flow rate of 500 ml/min.

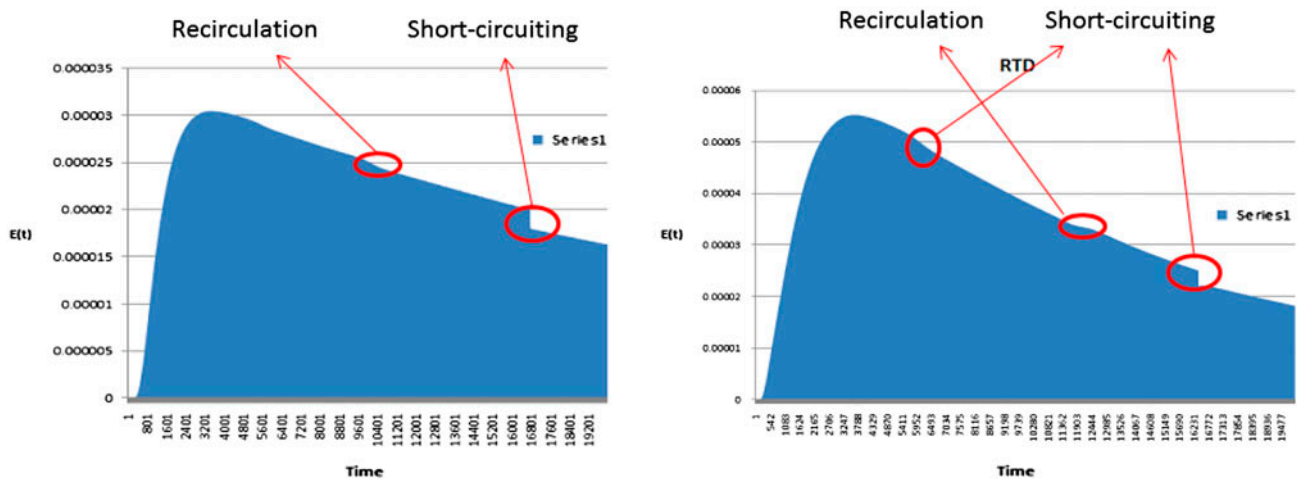


Fig. 19. Residence time distribution curves for square and triangle geometries, respectively, at a height of 31 cm and a flow rate of 150 ml/min.

$$t_{mean} = \frac{\int_0^\infty tCdt}{\int_0^\infty Cdt} \tag{7}$$

$$t_\theta = \frac{t_{mean}}{t_n} \tag{8}$$

where t_n is the minimal time, V_R is the volume of the wetland, V_0 is the inflow rate, t_{mean} is the mean time, C is the concentration of the impurity or the dye and t_θ is the normalized holding time [14,17,20].

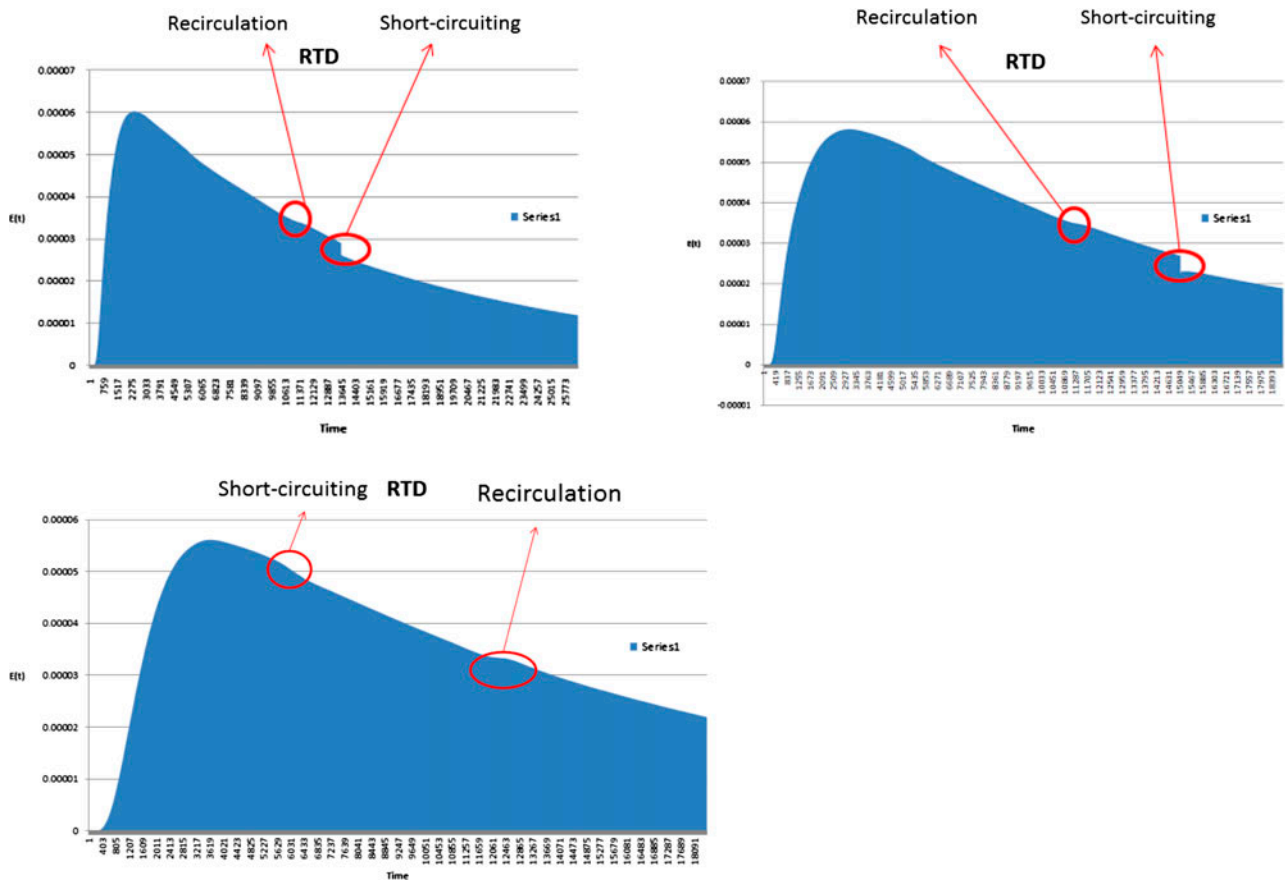


Fig. 20. Residence time distribution curves for the three geometries (square, square with two islands, and triangle, respectively) at a height of 31 cm and a flow rate of 300 ml/min.

To determine whether the flow in wetlands is close to plug or mixed flow, normalized variance is calculated [14,17]:

$$\sigma^2 = \frac{\int_0^\infty (t_{mean} - t)^2 E(t) dt}{\int_0^\infty E(t) dt} \tag{9}$$

$$\sigma_\theta^2 = \frac{\sigma^2}{t_n^2} \tag{10}$$

where σ is the variance, $E(t)$ is the residence time distribution function and σ_θ^2 is the normalized variance [17,20]. Hydraulic efficiency is calculated using the expression [14] (Table 1):

$$\lambda = t_\theta(1 - \sigma_\theta^2) \tag{11}$$

where λ is the hydraulic efficiency [14,17].

3. Models and dimensions

Different case study shapes and the different water heads and flow rates associated with each shape are shown below in Fig. 1 and Table 2, respectively.

4. Boundary conditions used in simulations

The pressure at the exit of each of the three wetland configurations illustrated in Fig. 1 is assumed to be 0 Pa. Flow through the porous medium is assumed to be unidirectional. Porous material is assumed to behave as a porous jump with an assumed permeability of $7.225 \times 10^{-9} \text{ m}^2$ [13]. The surface of the wetland open to the atmosphere is treated as a symmetric boundary condition [15]. No slip condition is assumed at the wetland walls in all the three wetland shapes presented in Fig. 1. No slip condition is also assumed to be valid on island or obstructions assumed within the wetland geometry. Wind and evapotranspiration effects are neglected.

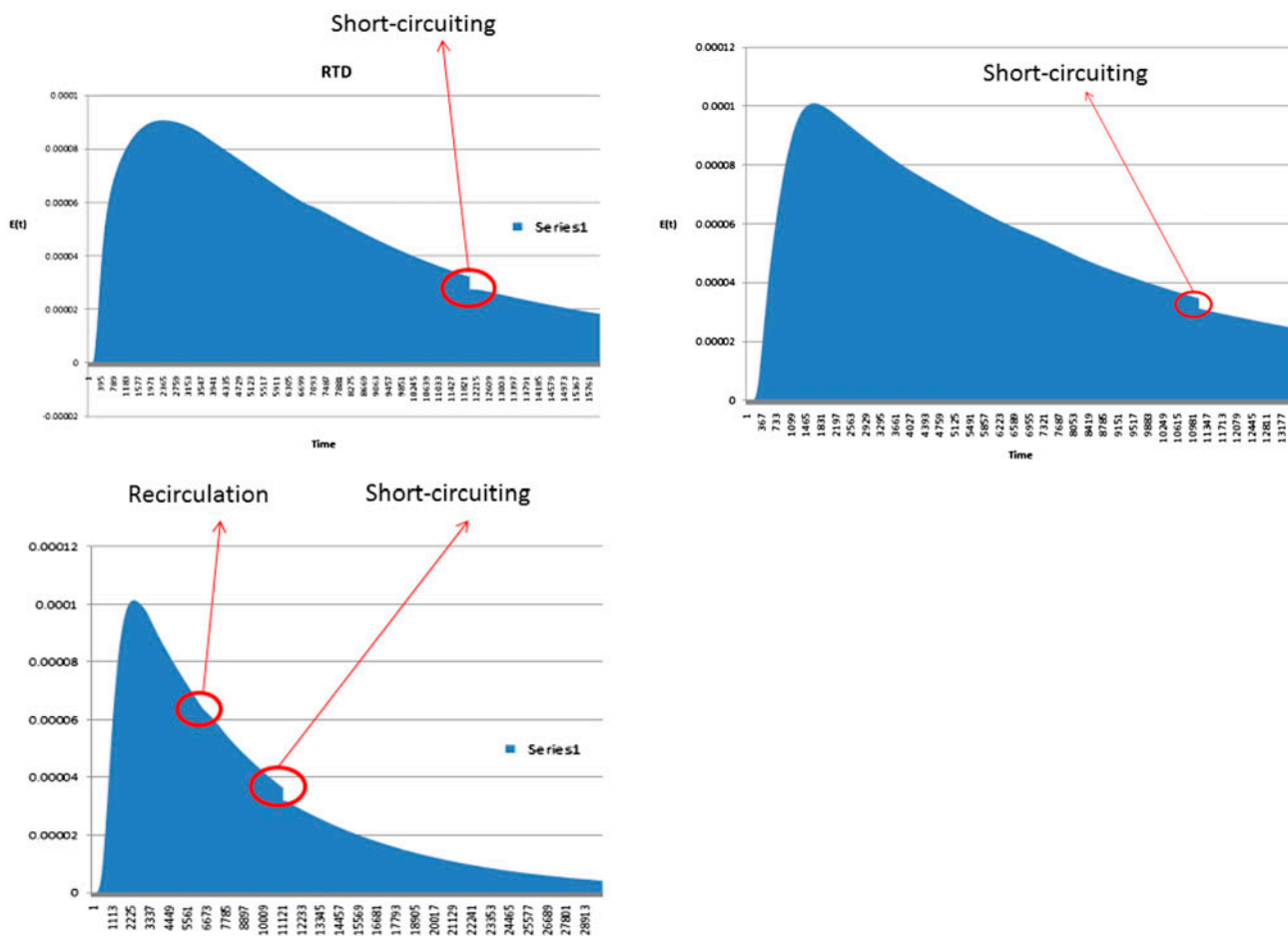


Fig. 21. Residence time distribution curves for the three geometries (square, square with two islands, and triangle, respectively) at a height of 31 cm and a flow rate of 500 ml/min.

5. Results and discussion

5.1. Hydrodynamic analysis of wetlands: 3D case studies

From Fig. 2, it is observed that at a flow rate of 150 ml/min, dead zones—portions with prominent water stagnation—are frequently formed. These portions are desirable as it will improve treatment efficiency of the wetlands, when compared with 500 ml/min where there is a considerable reduction in the dead zone volume due to high influent flux. The residence time of water will be less and hence, it will be not treated properly (Figs. 3 and 4).

When the height is increased to 31 cm, volume available for treatment increases. This will improve the residence characteristics. This also provides the organic-laden water or dye-laden water to interact with a larger wall surface area, which will provide an

overall increment in treatment as well as infiltration in practical wetland scenarios.

When the head of water within the wetland models simulated here is increased to 45.5 cm, it is observed that imminent mixing occurs and time spent by the fluid particles increases.

When the models having constructed islands or obstructions are simulated, it is observed that recirculation zones have considerably increased as shown in Fig. 5.

From Figs. 5–7, it can be observed that with the addition of islands, the probability of impurities to get caught in the recirculation zones and settle down or sediment due to very minimal speeds in flow may increase.

Recirculation zones in case of both the square model and the square with islands shape model

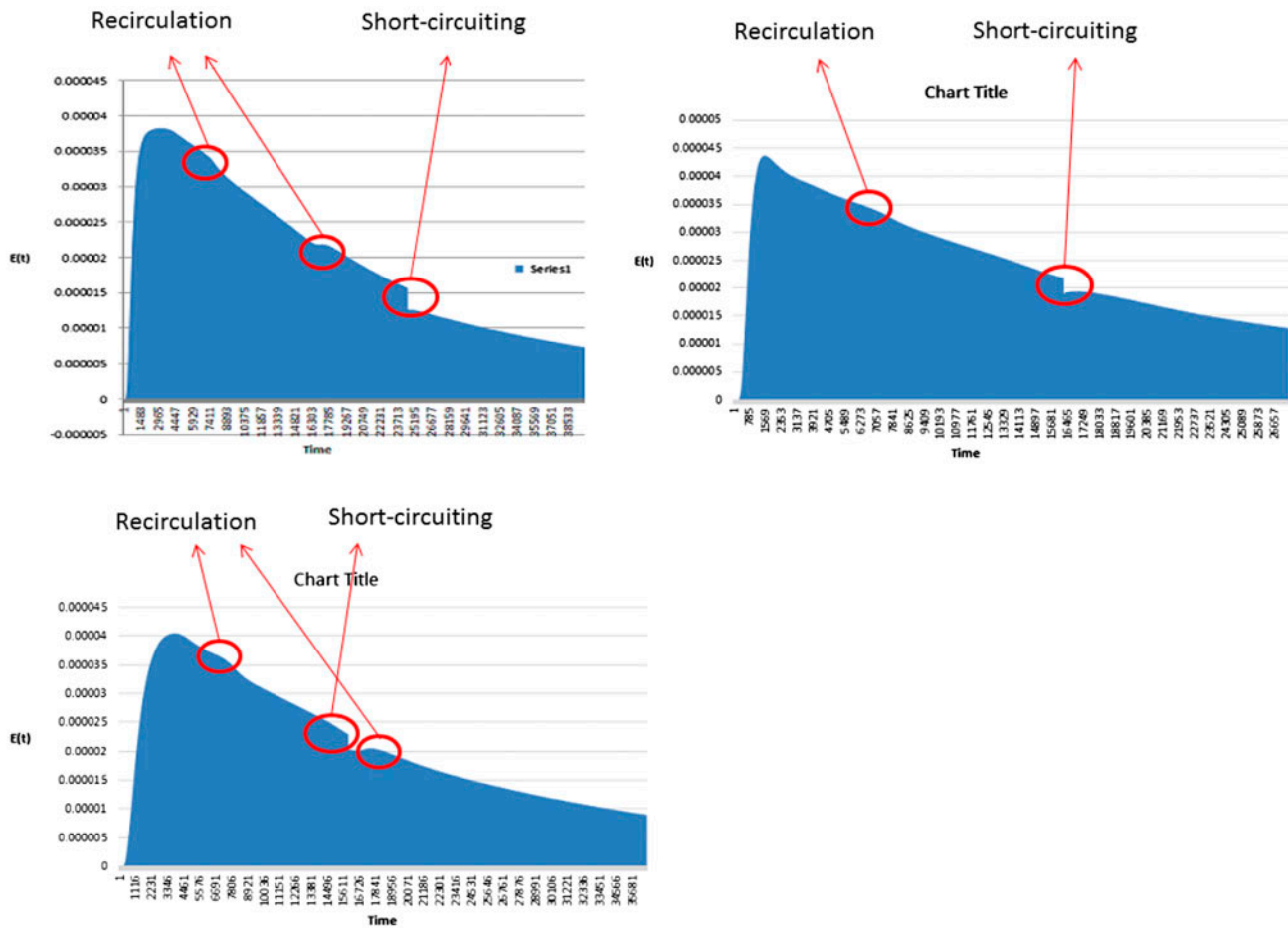


Fig. 22. Residence time distribution curves for the three geometries (square, square with two islands, and triangle, respectively) at a height of 45.5 cm and a flow rate of 300 ml/min.

decrease with increase in mass flow rates. But this is not the case with the triangular wetland model (Figs. 8–10).

A representative recirculation area was calculated by plotting the two-dimensional streamline plots of the three different cases discussed above on a square graph paper with square cells of equal areas and assessing the number of small squares encircled by the recirculation zones [15]. Using this crude two-dimensional visualization technique, the volume of dead zones for each shape was calculated. It is observed that the dead zone volume is minimal in case of a volumetric flow rate of 500 ml/min and increases with decrease in wetland inflow velocity. Similar result is also reiterated by the experimental results in Gupta et al. 2014. This is clearly illustrated in Fig. 11 at a specific depth of 15.5 cm. It is also observed that in a triangular model with a water depth of 15.5 cm, the recirculation area grows with velocity.

It is also observed from Figs. 11 and 12 that for a low head of 15.5 cm, at low inflow velocities of 150 ml/min, square recirculation was larger than the other two wetland shapes under consideration. It is also very pertinent to observe the fact that the recirculation areas for a flow of 150 ml/min through triangular and square with islands having the same bottom surface area remained approximately the same for both 15.5 and 31 cm deep water. It is also important to note that the area of recirculation in triangular wetlands increases with increase in velocity while it decreases with increase in velocity for square with island wetlands for flows at a depth of 15.5 cm.

Parameters like hydraulic efficiency and normalized variance can be used to determine the efficiency of the wetlands and how much time fluid particles have spent in the wetlands [17,20]. Table 3

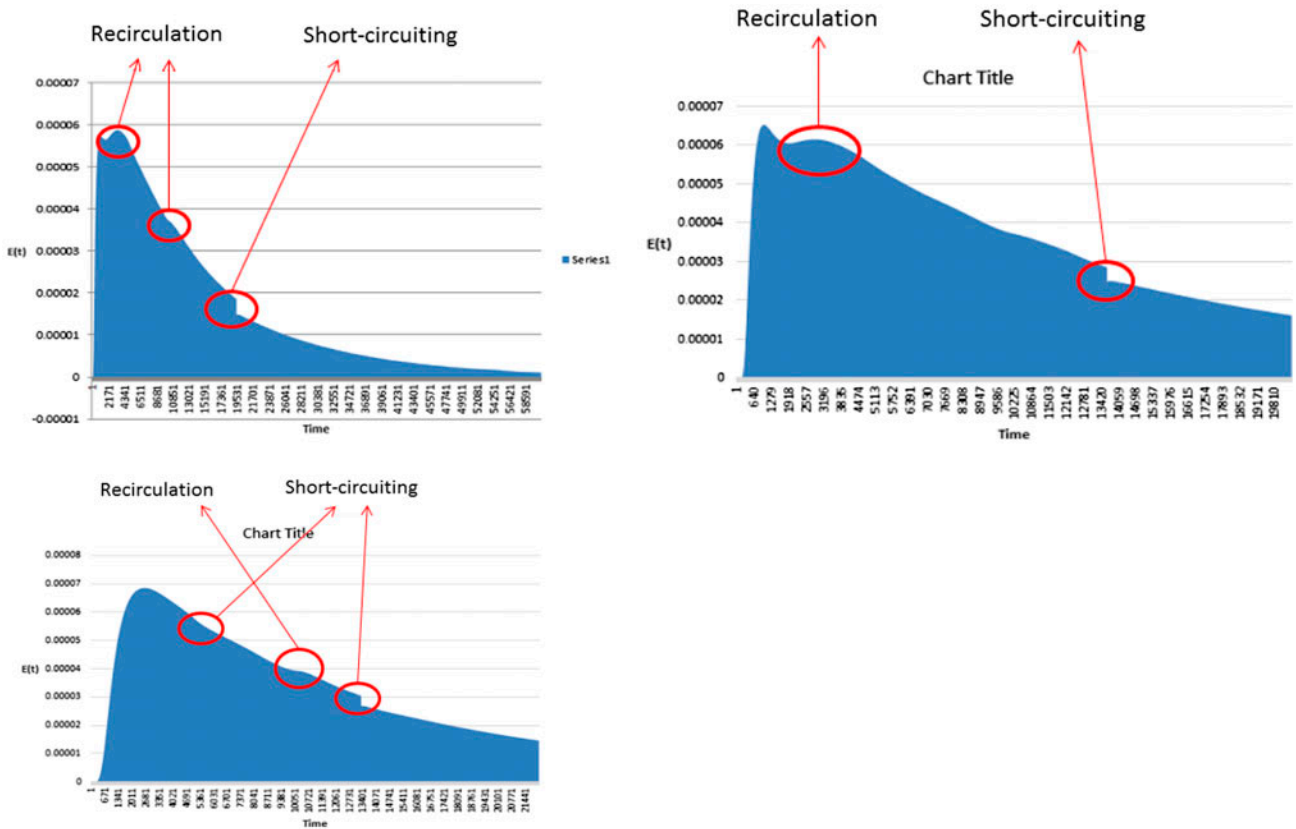


Fig. 23. Residence time distribution curves for the three geometries (square, square with two islands, and triangle, respectively) at a height of 45.5 cm and a flow rate of 500 ml/min.

Table 4

Coefficient of determination R^2 and error of the model S for predicting E-curve using $\frac{Y}{Y_{max}} = a + \frac{b_1 X_1}{X_{max}} + \frac{b_2 X_2}{X_{max}} + \frac{b_3 X_3}{X_{max}}$ for flow rate = 150 ml/min and height = 15.5 cm

Wetland model cases	a	b_1	b_2	b_3	R^2 (%)	S
Square	0.677	1.11	-5.23	3.66	78.2	0.1311
Square with two islands	0.1	3.15	-7.01	4.01	82.2	0.0593
Triangle	0.107	6.2	-14.1	8.21	87.1	0.101

shows the parameters calculated using the data obtained from the simulation results of Ansys Fluent™ 13.0 [19].

Fig. 13 shows the graph obtained between normalized variance and influent flow rate for square shaped wetland. It can be seen that the normalized variance is nearer to zero at a head of 31 cm and an inflow of 150 ml/min. This means that the flow is tending to a plug flow regime.

The plot between measure of mixing and flow for the square with island model is depicted in Fig. 14. With increase in velocity, an increase in mixing within the wetland is observed from this plot. This will increase the possibility of contact between impurities, and coalescence can happen easily, confirming an increase of hydraulic efficiency λ with increase in flow rate. This is also supported and illustrated by the increase in value of λ for the square with islands

Table 5

Coefficient of determination R^2 and error of the model S for predicting E-curve using $\ln Y = a + b_1X_1 + b_2X_2$ for flow rate = 300 ml/min and height = 15.5 cm

Wetland model cases	A	b_1	b_2	R^2 (in %)	S
Square	-43.6	-0.000074	4.56	49.2	2.2633
Square with two islands	-48.1	-0.000989	5.26	56.7	2.2589
Triangle	-37.1	-0.0044	3.5	54.1	1.751

Table 6

Coefficient of determination R^2 and error of the model S for predicting E-curve using $\frac{\ln X}{\ln Y} = a + b_1X_1 + b_2X_2$ for flow rate = 500 ml/min and a height = 15.5 cm

Wetland model cases	A	b_1	b_2	R^2 (in %)	S
Square	0.707	0.000048	-0.22	95	0.026
Square with two islands	0.948	0.000038	-0.242	96.1	0.0267
Triangle	0.863	0.000047	-0.238	95.1	0.02875

Table 7

Coefficient of determination R^2 and error of the model S for predicting E-curve using $\frac{\ln X}{\ln Y} = a + b_1X_1$ for flow rate = 150 ml/min and height = 31 cm

Wetland model cases	A	b_1	R^2 (in %)	S
Square	0.179	-0.113	91.2	0.03482
Square with two islands	0.0423	-0.102	84.9	0.04272
Triangle	-0.105	-0.0825	71.1	0.0524

Table 8

Coefficient of determination R^2 and error of the model S for predicting E-curve using $\frac{\ln X}{\ln Y} = a + b_1X_1$ for flow rate = 300 ml/min and height = 31 cm

Wetland model cases	A	b_1	R^2 (in %)	S
Square	-0.111	-0.826	74.9	0.04748
Square with two islands	0.0423	-0.102	84.9	0.04272
Triangle	-0.105	-0.0825	71.1	0.0524

Table 9

Coefficient of determination R^2 and error of the model S for predicting E-curve using $\frac{\ln X}{\ln Y} = a + b_1X_1$ for flow rate = 500 ml/min and height = 31 cm

Wetland model cases	a	b_1	R^2 (%)	S
Square	0.00174	-0.101	80	0.5002
Square with two islands	-0.1007	-0.0875	75.7	0.0492
Triangle	-0.364	-0.0536	37	0.067

Table 10

Coefficient of determination R^2 and error of the model S for predicting E-curve using $\frac{\ln X}{\ln Y} = a + b_1X_1 + b_2X_2$ for flow rate = 300 ml/min and height = 45.5 cm

Wetland model cases	a	b_1	b_2	R^2 (in %)	S
Square	0.370	0.000009	-0.146	96.6	0.01746
Square with two islands	0.328	0.00007	-0.140	74.2	0.0416
Triangle	0.406	0.000007	-0.149	97.3	0.0149

Table 11

Coefficient of determination R^2 and error of the model S for predicting E-curve using $\frac{\ln X}{\ln Y} = a + b_1X_1 + b_2X_2$ for flow rate = 500 ml/min and height = 45.5 cm

Wetland model cases	a	b_1	b_2	R^2 (in %)	S
Square	0.377	0.000013	-0.154	96.9	0.01663
Square with two islands	0.0785	0.000006	-0.112	91.2	0.017714
Triangle	0.406	0.000007	-0.149	97.3	0.0149

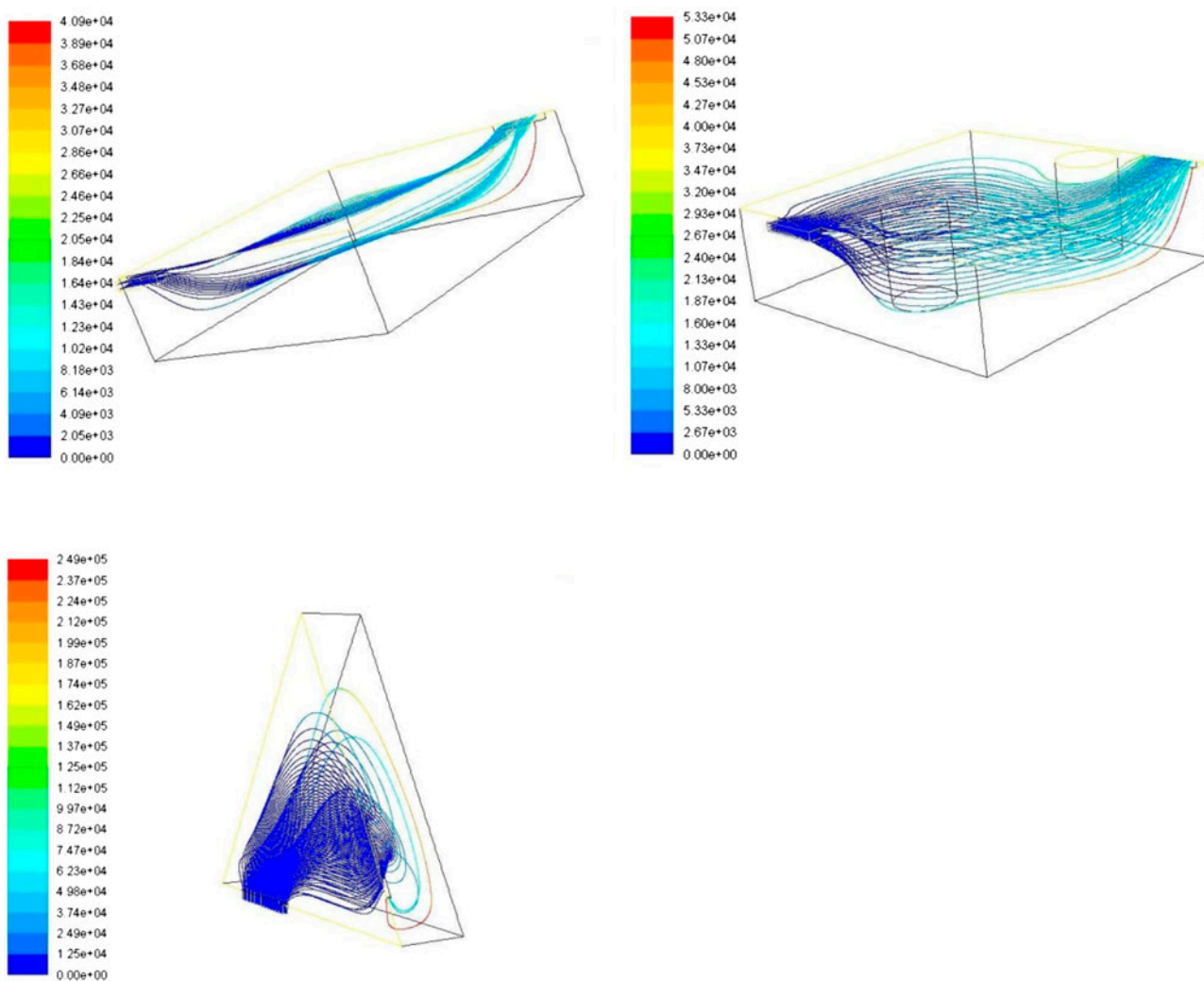


Fig. 24. Wood tracers through 15.5 cm deep constructed wetland models (square, square with two islands, and triangle, respectively) with glycerine inflow of 150 ml/min.

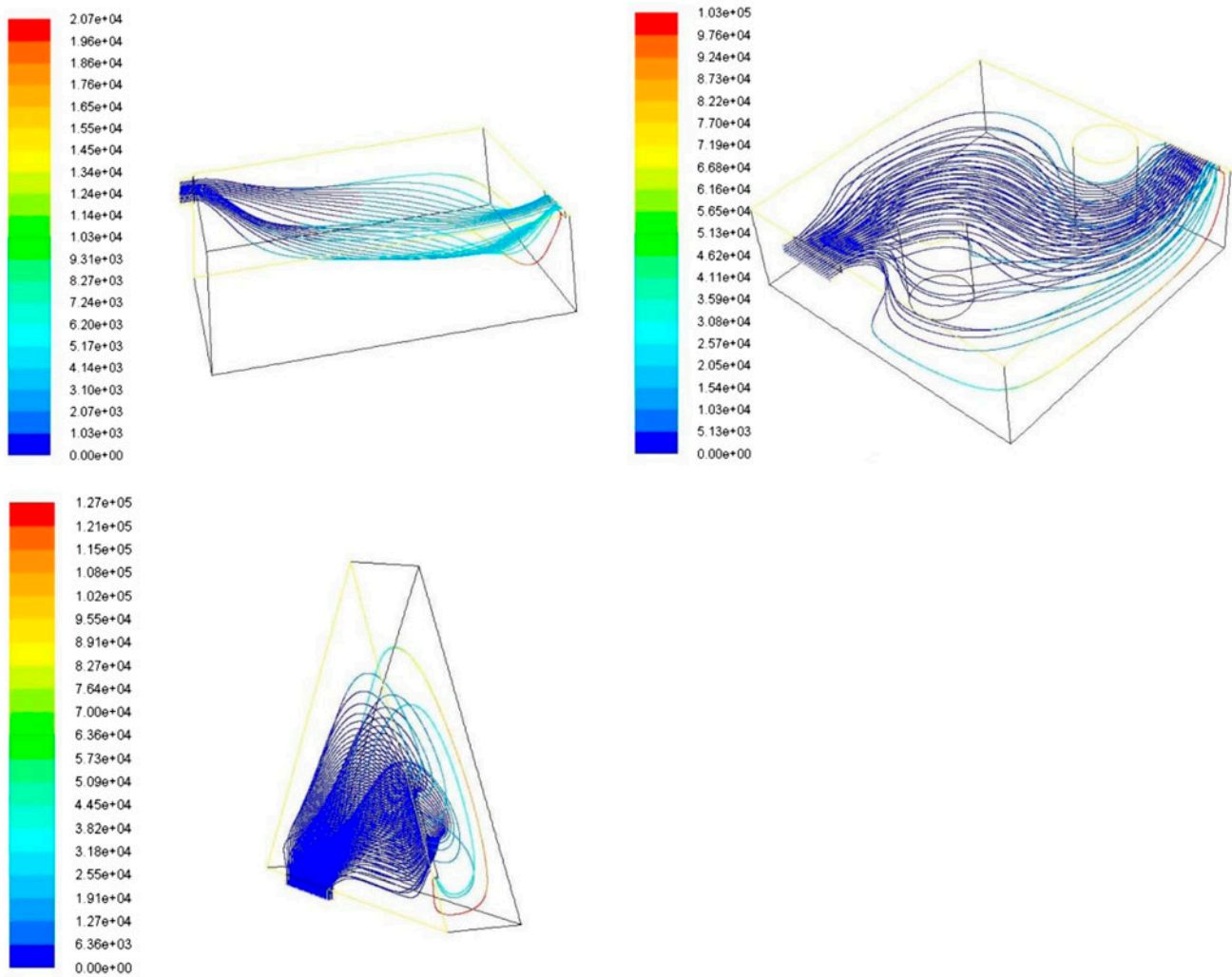


Fig. 25. Wood tracers through 15.5 cm deep constructed wetland models (square, square with two islands, and triangle, respectively) with glycerine inflow of 300 ml/min.

model for the cases of heads of water at 15.5, 31 and 45.5 cm, respectively. The highest value of λ was found to be 0.72 for the case of 500 ml/min flow rate at a head of 15.5 cm, indicating maximum occurrence of mixing [21].

A comparison of the results from Figs. 15 and 16 illustrates that the triangular shape provides a comparatively higher pace of mixing when compared with the square with islands model for a head of 31 cm. It is also noted that the lowest λ values in all the case studies occur with 15.5 head and 31.0 cm head in the triangular shape model. This means that least mixing is observed in these cases, and the flow is close to plug flow

when compared with all the other experiments performed.

6. Residence time distribution curves

Residence time distribution curves from Figs. 15–23 are plotted from the data obtained through simulations using Ansys Fluent. From these residence time distribution curves, it can be known whether short-circuiting happens in the wetlands or whether there are any recirculation zones present in the wetlands [17]. The following figures show the recirculation zones for each shape.

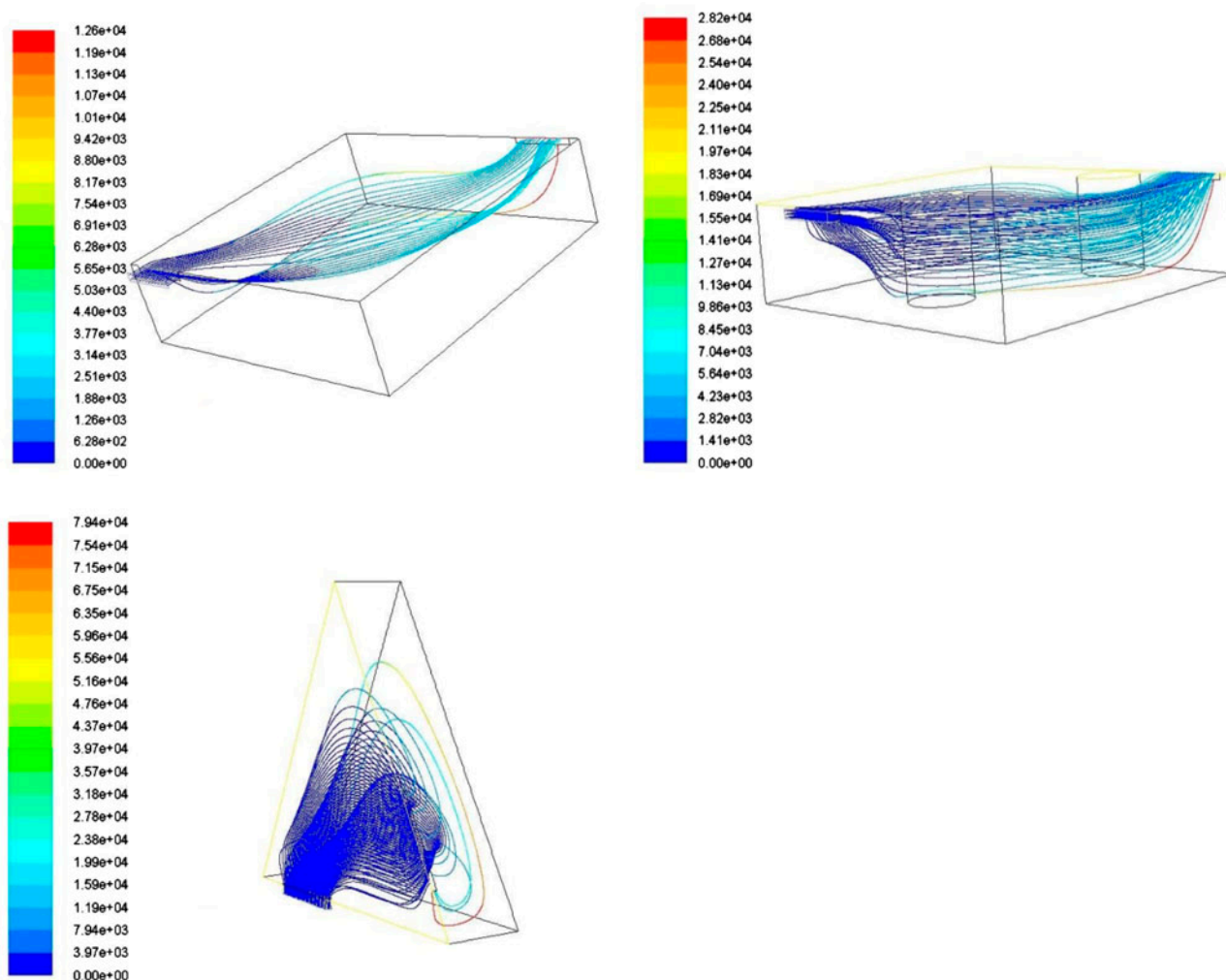


Fig. 26. Wood tracers through 15.5 cm deep constructed wetland models (square, square with two islands, and triangle, respectively) with glycerine inflow of 500 ml/min.

Using the compartment model theory in Figs. 15–23, it is found that there is some short-circuiting, and some recirculation zones are present in these shapes of the wetlands for the flow and the height parameters used [17].

7. Regression modelling

From the residence time distribution (RTD) data derived from the graphs and earlier discussions it is observed that there is more than one variable affecting the RTD function. Therefore, the RTD or E value can be derived using stochastic multi-parameter approach [22]. The residence time plots from Figs. 15–23 represent a polynomial distribution. Therefore, the

multi-parameter model for each shape (square, square with two islands, and triangle, respectively) can be expressed as follows:

$$\frac{Y}{Y_{max}} = a + \frac{b_1 X_1}{X_{max}} + \frac{b_2 X_2}{X_{max}^2} + \frac{b_3 X_3}{X_{max}^3} \quad (12)$$

where Y is normalized mole fraction and Y_{max} is the maximum value of the normalized mole fraction of species. Assume X_1 is t , X_2 is t^2 , X_3 is t^3 and X_{max} is t_{max} . Eq. (12) is a non-dimensional framework and regression may be performed to predict the E-curve. Table 4 presents the regression fits for three different constructed wetland models with a depth of 15.5 cm and an inflow of 150 ml/min.

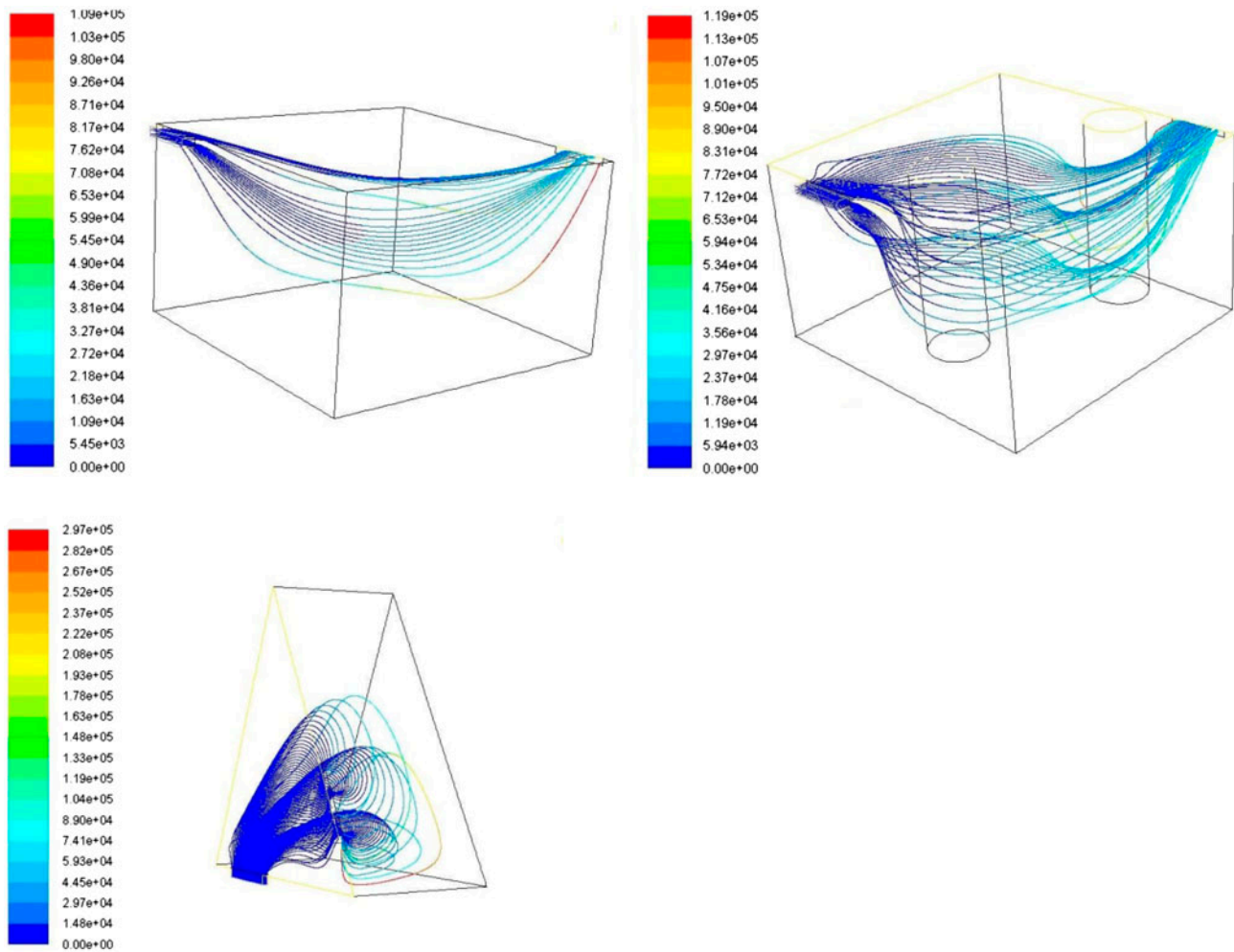


Fig. 27. Wood tracers through 31 cm deep constructed wetland models (square, square with two islands, and triangle, respectively) with glycerine inflow of 150 ml/min.

A separate fit formulation is used to characterize a flow rate of 300 ml/min and a depth of 15.5 cm. The model for the variation in the residence time distribution function as a nonlinear function is given as

$$\ln Y = a + b_1 X_1 + b_2 X_2 \quad (13)$$

where Y is the normalized mole fraction, X_1 is t and X_2 is $\ln t$. Table 5 presents the regression fits for the three different constructed wetland models with a depth of 15.5 cm and an inflow of 300 ml/min.

A new model fit is utilized to characterize an inflow rate of 500 ml/min and a depth of 15.5 cm. The multi-parameter model for variation in the

residence time distribution function as a function of time with the model take the form,

$$\frac{\ln X_1}{\ln Y} = a + b_1 X_1 + b_2 X_2 \quad (14)$$

where Y is the normalized mole fraction, X_1 is t and X_2 is $\ln t$. Table 6 presents the regression fits for the three different constructed wetland models with a depth of 15.5 cm and an inflow of 500 ml/min.

A new fit is formalized to represent the case of an inflow rate of 150 ml/min through the wetland geometries with a depth of 31 cm. Variation in the residence time distribution function Y is predicted using the expression,

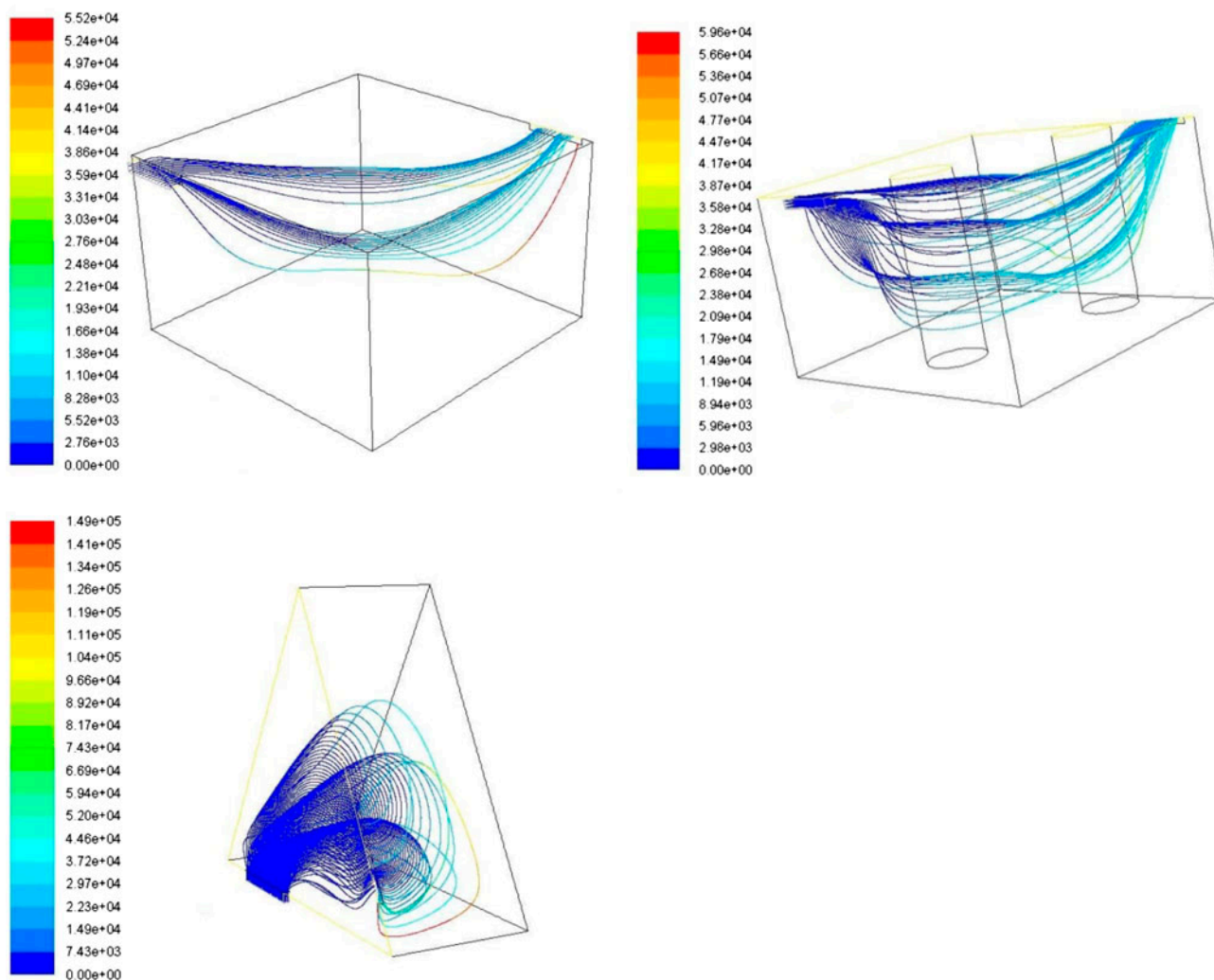


Fig. 28. Wood tracers through 31 cm deep constructed wetland models (square, square with two islands, and triangle, respectively) with glycerine inflow of 300 ml/min.

$$\frac{\ln X_1}{\ln Y} = a + b_1 X_1 \tag{15}$$

where Y is the normalized mole fraction, and X_1 is $\ln t$. Table 7 presents the regression fits for the three different constructed wetland models with a depth of 31 cm and an inflow of 150 ml/min.

A similar modelling strategy is used to predict the E-curve in the case of flow rate of 300 ml/min passing through wetlands with a depth of 31 cm. The prediction model for the residence time distribution function takes the form of Eq. (15). Table 8 presents the regression fits for the three different constructed wetland

models with a depth of 31 cm and an inflow of 300 ml/min.

Eq. (15) is found to be a good predictor of the E-curve in case of wetland geometries with an inflow rate of 500 ml/min and a depth of 31 cm. Table 9 presents the regressions equations for the distinct wetland geometries studied with a depth of 31 cm and inflow of 500 ml/min.

Eq. (14) is utilized to fit a prediction equation for 45.5 cm deep constructed wetland models with a dye-laden inflow at the rate of 300 ml/min. Table 10 presents the coefficient of determination and error of this fit. Here, Y is the normalized mole fraction, X_1 is t and X_2 is $\ln t$.

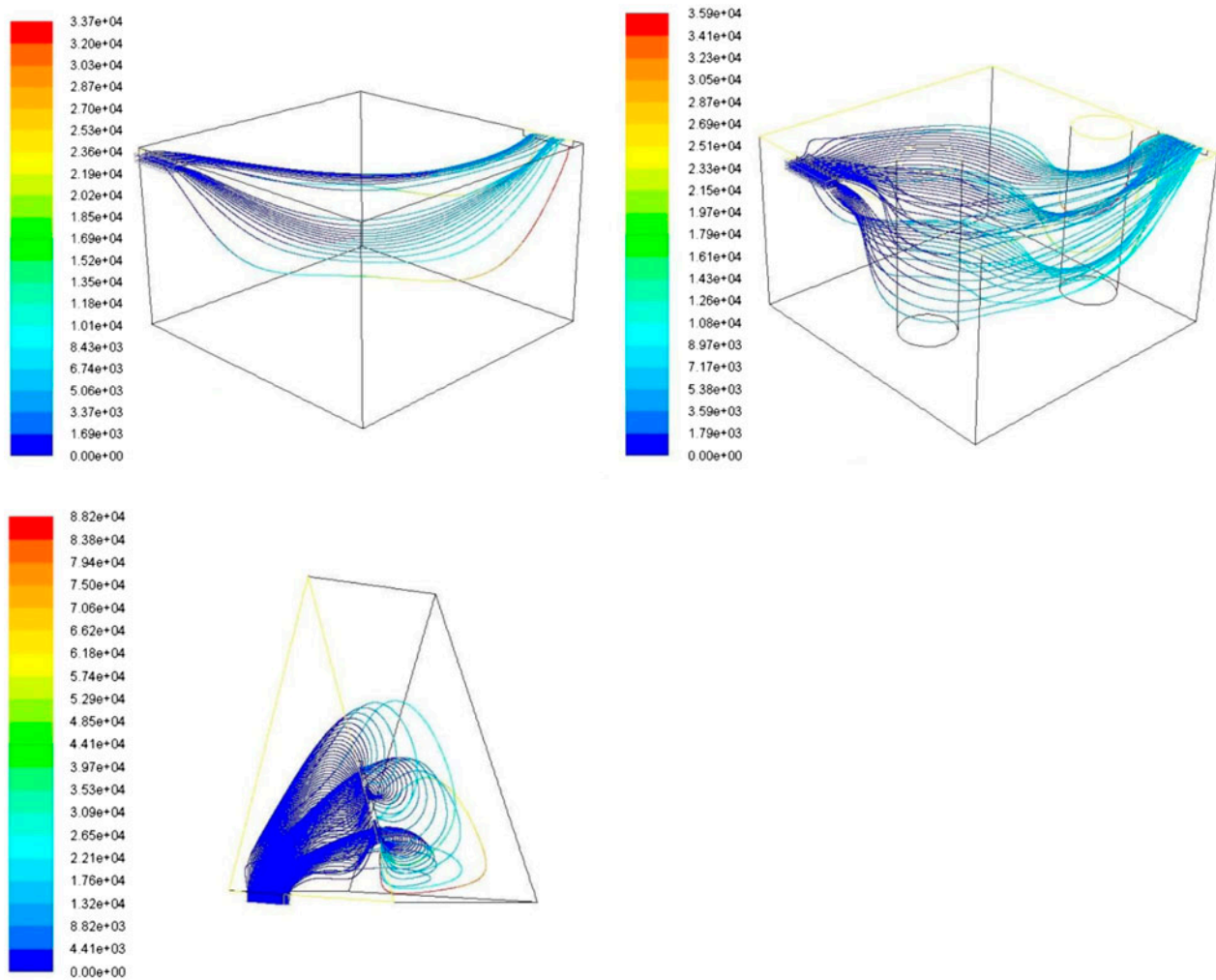


Fig. 29. Wood tracers through 31 cm deep constructed wetland models (square, square with two islands, and triangle, respectively) with glycerine inflow of 500 ml/min.

Dye-laden flows of 500 ml/min through the three different constructed wetland geometries discussed in this article with a water depth of 45.5 cm can be characterized using Eq. (14). Table 11 illustrates the coefficients of the model, its degree of prediction and its error. Here, Y is the normalized mole fraction, X_1 is t and X_2 is $\ln t$.

8. Residence time distribution of sewage simulated using Glycerol

Glycerine has the same viscosity as sewage water [16]. To determine how waste (dyes and particles) in sewage water moves, simulations using glycerine with wood particles immersed in it are carried out. Here, wood particles denote waste matter

flowing in sewage water. The figure below shows the path and residence time of these wood particles in glycerine.

From the above tracer imageries in Figs. 24–30, it is observed that a non-intermixing flow occurs, relating the flow to a plug type. It is also seen that the tracer dyes are restricted to a specific region within the sewage flow which also indicates low dispersion of dye-based impurities within sewage. This indicates a major problem in treating sewage with flowing dye concentrations. From the above figures, it can be also concluded that the residence distribution time of wood particles in glycerine increases with the addition of islands and the residence time also increases with increase in wetland depth.

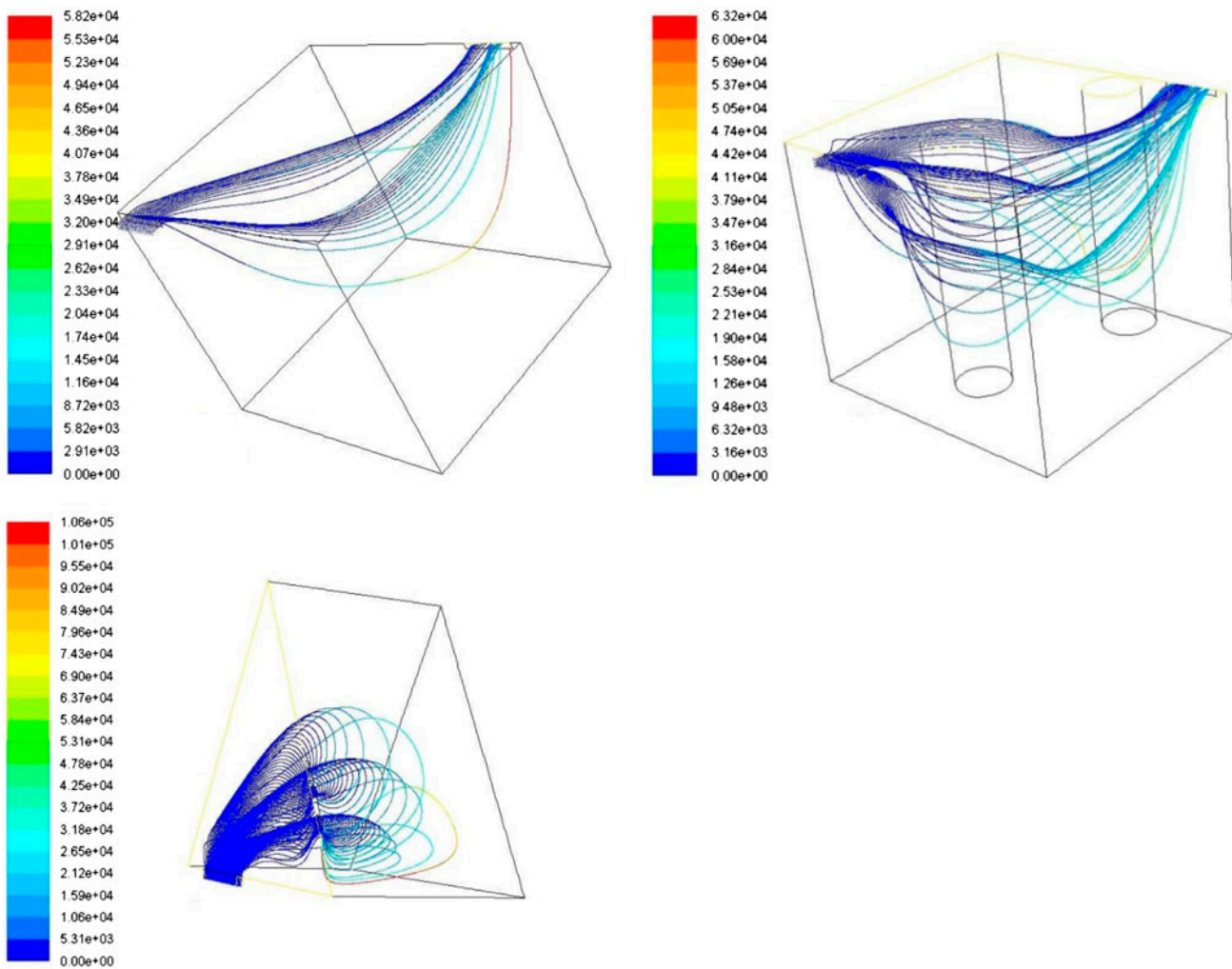


Fig. 30. Wood tracers through 45.5 cm deep constructed wetland models (square, square with two islands, and triangle, respectively) with glycerine inflow of 500 ml/min.

9. Conclusion

Increasing velocities enhances mixing in the wetlands analysed in this document. This is also confirmed by an increase of hydraulic efficiency λ with increase in flow rate. The highest value of λ was found in case of the 500 ml/min flow rate in a wetland 15.5 cm deep. This is a phenomenon showing the importance of shallow wetlands with high inflow rates. For this depth, the area of recirculation in triangular wetlands increases with increase in velocity, while it decreases with increase in velocity for square wetlands with constructed islands or obstructions.

In general, recirculation volume is minimal at high flow rates and increases with decrease in wetland inflow velocities. A medium depth (31 cm) wetland

residence time distribution function prediction single-parameter model is developed. For this depth, the triangular shape provides a comparatively higher pace of mixing when compared with the square with islands model. A single equation multi-parameter model is developed for the prediction of E-curve for 15.5 and 45.5 cm deep wetland model configurations, respectively.

In case of high-density flows such as sewage flow, no mixing takes place, and plug flows are prominent, irrespective of the depth of the wetland. Here, glycerine flow simulates the sewage flows in the wetlands and improvement in residence time may be probable with the construction of obstructions and increasing wetland depth.

Acknowledgements

The authors would like to thank Mr Ganpat Choudhary and Mr Mahesh from the Chemistry laboratory at IIT Jodhpur. The authors would also thank the administration of IIT Jodhpur for providing seed grant Project No. IITJ/SEED/20140002 support in 2014.

References

- [1] Available from: <http://wgbis.ces.iisc.ernet.in/energy/water/paper/wetlands/impacts.html#1>.
- [2] W.J. Mitch, J.G. Gosselink, Wetlands, Van Nostrand Reinhold, New York, NY, 1986.
- [3] R.H. Kadlec, S.D. Wallace, Treatment Wetlands. second ed., CRC Press, New York, NY, 2009.
- [4] A.K. Plappally, J. Lienhard V, Energy requirements for water production, treatment, end use, reclamation, and disposal, Renew. Sust. Energ. Rev. 16(7) (2012) 4818–4848.
- [5] N. Gollehen, W. Quinby, Water and Wetlands Resources, in: K. Weibe and N. Gollehen (Eds.), Agricultural Resources and Environmental Indicators, Nova Science, New York, NY, 2006, pp. 23–32.
- [6] A.K. Plappally, J.H. Lienhard, Costs for water supply, treatment, end-use and reclamation, Desalin. Water Treat. 51 (2013) 200–232.
- [7] R.H. Liwei Fan, Z. Lu, CFD, study on hydraulic performance of subsurface flow constructed wetland: Effect of distribution and catchment area, Korean J. Chem. Eng. 26(5) (2009) 1272–1278.
- [8] L. Fan, H. Reti, W. WANG, Z. LU, Z. Yang, Application of computational fluid dynamic to model the hydraulic performance of subsurface flow wetlands, J. Environ. Sci. 20(12) (2008) 1415–1422.
- [9] J. Persson, The hydraulic performance of ponds of various layouts, Urban Water 2 (2000) 243–250.
- [10] X. Wei, X. Wang, B. Dong, X. Li, A.K. Plappally, Z. Mao, L.C. Brown, Simplified residence time prediction models for constructed wetland water recycling systems, Desalin. Water Treat. 51(7–9) (2013) 1494–1502.
- [11] X. Wei, A.K. Plappally, L.C. Brown, A.B.O. Soboyejo, B. Dong, Z. Mao, Numerical and multivariate stochastic approaches to characterize guilin wetland dynamics, Stoch. Environ. Res. Risk Assess. 25(8) (2011) 545–556. doi:10.1007/s00477-011-0520-6.
- [12] H. Versteeg, W. Malalasekera, An Introduction to Computational Fluid Dynamics The Finite Volume Method, John Wiley & Sons, New York, NY, 1995.
- [13] UCD, Momentum Equations for Porous Media. Available from: http://aerojet.engr.ucdavis.edu/fluent_help/html.
- [14] Z.L. Liwei Fan, R. Hai, CFD study on hydraulic performance of subsurface flow constructed wetland: Effect of distribution and catchment area, Korean J. Chem. Eng. 26(5) (2009) 1272–1278.
- [15] A.K. Plappally, M.A.R. Sharif, R.C. Bradt, Modelling the flow of molten steel in a Tundish containing an inclusion filtering trap, Fluid Dyn. Mater. Process. 3 (2007) 115–128.
- [16] W.D. Hatfield, The viscosity or pseudo-plastic properties of sewage sludges, Sewage Works J. 10(1) (1938) 3–25.
- [17] O. Levenspiel, Chemical Reaction Engineering, third ed., Wiley, New York, NY, 1999.
- [18] Fluent, Discrete phase models, in: Fluent Manual, Fluent Inc., 2005, 23-1–23-170 (Chapter 23). Available from: <http://cdlab2.fluid.tuwien.ac.at/LEHRE/TURB/Fluent.Inc/fluent6.2/help/pdf/ug/chp23.pdf>.
- [19] G.O. Schwab, D.D. Fangmeier, W.J. Elliot, S.R. Workman, G.O. Schwab, Soil and Water Conservation Engineering, fifth ed., ASABE, Boston, MA, 2011.
- [20] G.O. Schwab, D.D. Fangmeier, W.J. Elliot, Soil and Water Conservation Engineering, ASABE, Boston, MA, 2011.
- [21] S. Gupta, R. Singh, P.R. Chakraborty, R.K. Sharma, A.B.O. Soboyejo, X. Wei, A. Plappally, Multi-variable approach to determine treatment efficiency of wetland: Size Effect and Electro-Kinetic Effects, Desalin. Water Treat. (2014), in press.
- [22] A. Plappally, Theoretical and Empirical Modelling of Flow, Strength, Leaching and Micro Structural Characteristics of V Shaped Porous Ceramic Water Filters, PhD Dissertation, 2010.